Understanding the Role of Ocean Dynamics in Midlatitude Sea Surface Temperature Variability using a Simple Stochastic Climate Model

Casey R. Patrizio* David W.J. Thompson

Department of Atmospheric Sciences, Colorado State University, Ft. Collins, Colorado, USA.

*Corresponding author: Casey Patrizio, casey.patrizio@colostate.edu

Early Online Release: This preliminary version has been accepted for publication in *Journal of Climate* be fully cited, and has been assigned DOI 10.1175/JCLI-D-21-0184.1. The final typeset copyedited article will replace the EOR at the above DOI when it is published.

ABSTRACT

In a recent paper, we argued that ocean dynamics increase the variability of midlatitude sea-surface temperatures (SST) on monthly to interannual timescales, but act to damp lower-frequency SST variability over broad midlatitude regions. Here, we use two configurations of a simple stochastic climate model to provide new insights into this important aspect of climate variability. The simplest configuration includes the forcing and damping of SST variability by observed surface heat fluxes only, and the more complex configuration includes forcing and damping by ocean processes, which are estimated indirectly from monthly observations. It is found that the simple model driven only by the observed surface heat fluxes generally produces midlatitude SST power spectra that are too *red* compared to observations. Including ocean processes in the model reduces this discrepancy by *whitening* the midlatitude SST spectra. In particular, ocean processes generally increase the SST variance on < 2 year timescales, and decrease it on > 2 year timescales. This happens because oceanic forcing increases the midlatitude SST variance across many timescales, but oceanic damping outweighs oceanic forcing at timescales > 2 years, particularly away from the western boundary currents. The whitening of midlatitude SST variability by ocean processes also operates in NCAR's Community Earth System Model (CESM). That is, midlatitude SST spectra are generally redder when the same atmospheric model is coupled to a slab rather than dynamically-active ocean model. Overall, the results suggest that forcing and damping by ocean processes play essential roles in driving midlatitude SST variability.

Accepted for publication in *Journal of Climate*. DOI 10.1175/JCLI-D-21-0184.1.

1. Introduction

The role of ocean dynamical processes in midlatitude sea surface temperature (SST) variability is an important aspect of midlatitude climate variability, but remains incompletely understood. In this study, we provide insights into this key issue using a simple stochastic climate model that includes parameterizations of both the forcing and damping of SST variability by ocean processes.

In the stochastic climate model framework (Hasselmann 1976; Frankignoul and Hasselmann 1977), fluctuations in SSTs are generally interpreted as the response of the ocean mixed-layer to random atmospheric variability (i.e. white-noise). In one of the simplest formulations of the model, the SST anomalies, T', are forced by atmospheric variability through turbulent and radiative heat fluxes at the sea surface, F_a, and are linearly damped by $-\lambda_s T'$, which parametrizes the damping due to the surface heat flux feedback. In the model, the high-frequency component of atmospheric variability is damped by the large heat capacity of the ocean mixed-layer, C_o, such that the resulting SST variability has a redder spectrum than the atmospheric forcing. Despite its simplicity, the stochastic climate model has been shown to capture some key aspects of midlatitude SST variability, such as the shape of the power spectrum of midlatitude SSTs (e.g. Frankignoul and Hasselmann 1977; Frankignoul 1979) and the covariability between SSTs and the surface heat fluxes (e.g. Frankignoul et al. 1998). As such, this model can be viewed as a “null hypothesis" for SST variability, particularly in midlatitude regions where atmospheric weather drives large variations in the surface heat fluxes.

A more realistic model of the mixed layer can be formed by extending the stochastic climate model to allow temperatures in the atmosphere and ocean to respond to each other through surface heat exchange (Barsugli and Battisti 1998). The thermodynamic coupling between atmosphere

Accepted for publication in *Journal of Climate*. DOI 10.1175/JCLI-D-21-0184.1.

and ocean-surface temperatures leads to "reduced thermal damping", which further reddens the variability of SSTs compared to uncoupled stochastic climate model.

Whether coupled or uncoupled these simple models of climate variability can be considered to be 'passive ocean models' in that they do not explicitly include ocean dynamical processes. Such models form the basis for the widely held notion that midlatitude SST variability is driven primarily by atmospheric processes. However, such models are also known to be deficient in some regions. For example, previous studies have shown that the stochastic climate model simulates closely the observed SST power spectra in the Northeast Pacific, but do not closely reproduce the observed spectra in regions with more active ocean dynamics, such as in the western boundary currents or around the North Atlantic subpolar gyre (e.g. Reynolds 1978; Hall and Manabe 1997; Zhang 2017).

The role of ocean dynamical processes in midlatitude SST variability has been explored in many studies. Deser et al. (2003) demonstrated that the stochastic climate model more accurately captures the persistence of winter SSTs from one year to the next throughout the North Atlantic and North Pacific when seasonal variations in vertical entrainment are accounted for in the model formulation. Roberts et al. (2017) and Patrizio and Thompson (2021) estimated the ocean heat flux convergence as a residual in the mixed layer energy budget, and showed that ocean processes play an important role in driving monthly to interannual variability of upper-ocean temperatures in the western boundary currents, their eastward extensions, and the Antarctic circumpolar current. Broadly similar conclusions were reached by Bishop et al. (2017) who used an extended Barsugli and Battisti (1998) model with stochastic oceanic forcing to interpret the observed relationships between the surface heat fluxes and SSTs. Similar results have also been derived from direct estimates of the heat transport in the ocean mixed layer obtained from observation-assimilating ocean models (e.g. Buckley et al. 2014, 2015; Patrizio and Thompson 2021). And numerous

Accepted for publication in *Journal of Climate*. DOI 10.1175/JCLI-D-21-0184.1.

studies have shown that mesoscale ocean dynamics play an important role in driving midlatitude atmosphere-ocean interactions in both observations (e.g. Small et al. 2008; Frenger et al. 2013; Ma et al. 2015) and global climate models (e.g. Kirtman et al. 2012; Ma et al. 2016; Siqueira and Kirtman 2016; Putrasahan et al. 2017; Saravanan and Chang 2019; Small et al. 2019a,b; Bellucci et al. 2020).

In general, there have been substantial improvements in our understanding of the role of midlatitude ocean dynamics in midlatitude SST variability on month-to-month and interannual timescales. However the picture is much more unclear at lower-frequencies. In large part, this is due to the limitations of observations and uncertainties in simulations of ocean dynamics on, say, decadal timescales. Consider, for example, the most prominent patterns of low-frequency SST variability in the extratropics: Pacific Decadal Variability (PDV) and Atlantic Multidecadal Variability (AMV). While there is general consensus that both atmospheric and oceanic processes contribute to PDV, the relative roles of both processes are unclear (e.g Alexander et al. 2002; Newman et al. 2003; Deser et al. 2004; Kwon and Deser 2007; Alexander et al. 2010; Newman et al. 2016; Wills et al. 2019b). The picture is even less clear for AMV. Some studies have argued that AMV is driven primarily by atmospheric processes, including internal atmospheric variability (e.g. Clement et al. 2015; Cane et al. 2017) and external radiative forcing (e.g. Murphy et al. 2017; Bellomo et al. 2018; Murphy et al. 2021). Other studies have argued that AMV is fundamentally dependent on ocean processes, particularly those associated with the Atlantic meridional overturning circulation (AMOC) (e.g. Zhang and Wang 2013; Buckley and Marshall 2016; O'Reilly et al. 2016; Delworth et al. 2017; Zhang 2017; Kim et al. 2018; Yan et al. 2018; Wills et al. 2019a; Zhang et al. 2019).

In our recent paper (Patrizio and Thompson 2021; hereafter PT21), we quantified the role of ocean dynamics in two ways: 1) indirectly from observations of surface heat fluxes and SSTs, and 2) directly using output from the Estimating the Circulation and Climate of the Ocean (ECCO)

Accepted for publication in *Journal of Climate*. DOI 10.1175/JCLI-D-21-0184.1.

project. A key result is that the ocean dynamical contribution to SST variance generally decreases with timescale in many midlatitude regions. In fact, ocean dynamics act to *reduce* the SST variance on timescales longer than a few years over much of the Northern Hemisphere oceans. The period of record used in the analysis was not long enough to draw definitive conclusions about the role of ocean dynamics on decadal and greater timescales. However, the results strongly suggest that the midlatitude ocean acts to damp rather than force SST variability on the low-frequency timescales resolvable in the satellite era.

The purpose of this study is to provide further insights into the role of ocean dynamics in midlatitude SST variability using two different configurations of a simple stochastic climate model. In the simplest configuration the model is driven by surface heat fluxes only (black terms in Figure 1), and in the more complex configuration the model is extended to include both the forcing (F_o) and damping (λ_o) of SST variability by ocean processes (red terms in Figure 1). Ocean processes have been included in previous simple models of midlatitude climate variability (e.g. Frankignoul and Reynolds 1983; Frankignoul 1985; Frankignoul et al. 1998; Alexander and Penland 1996; Hall and Manabe 1997; Wu et al. 2006; Qiu et al. 2007; Bishop et al. 2017; Cane et al. 2017; Zhang 2017). However, here we use a novel approach to estimate the ocean dynamical terms from observationally-based data and, in turn, draw novel conclusions about the role of ocean dynamics in midlatitude SST variability. The goal of this work is to provide a broad perspective on the relative roles of the ocean dynamical forcing and damping terms in midlatitude climate variability, rather than to understand the detailed ocean physics behind each term. The conclusions are tested in output from an atmospheric general circulation model coupled to a dynamically-active ocean model (hereafter referred to as the fully-coupled model) and a slab-ocean model using NCAR's Community Earth System Model (CESM1; Hurrell et al. 2013).

Accepted for publication in *Journal of Climate*. DOI 10.1175/JCLI-D-21-0184.1.

The key results are that 1) the simple stochastic climate model driven solely by the observed surface heat fluxes yields midlatitude SST power spectra that are much redder than observed midlatitude SST power spectra, 2) the inclusion of both oceanic forcing *and* oceanic damping terms in the simple model reduces the discrepancy with observations by decreasing the low-frequency SST variance and increasing the high-frequency SST variance, and 3) the resulting "whitening" of midlatitude SST variability by ocean dynamics is also apparent in the differences between SST variability in slab-ocean and fully-coupled configurations of CESM.

Methods and data are described in Section 2, results are shown in Section 3, and conclusions are provided in Section 4.

2. Data & Methods

This section is divided into four parts. Section 2a reviews the data sources used in the analyses. Section 2b describes the stochastic climate model. Section 2c outlines the methods used for estimating the oceanic forcing and damping terms in the model. Section 2d provides a derivation of the SST power spectrum of the model.

a. Observational data sources and model output

The primary observational data sources are objectively-analyzed surface turbulent heat fluxes (latent and sensible) and SSTs from OAFlux (Yu et al. 2008), and surface radiative heat fluxes and wind stress from the MERRA-2 reanalysis product (Gelaro et al. 2017). The OAFlux SSTs are from the NOAA Optimum Interpolation (OI) 0.25° SST analysis produced by Reynolds et al. (2007) that has been averaged onto a 1° degree grid. In all cases, monthly-mean data are used over the period 1980-2017 and at 1° resolution. We use the OAFlux product since it provides global coverage of the air-sea heat fluxes across multiple decades and is derived using state-of-the-art bulk

Accepted for publication in *Journal of Climate*. DOI 10.1175/JCLI-D-21-0184.1.

flux parameterizations (Yu et al. 2008). To calculate the monthly anomalies, we remove both the linear trend and seasonal cycle from the SSTs and air-sea heat fluxes prior to all analyses.

Following PT21, the observations are used to estimate monthly anomalies in the ocean mixed-layer heat flux convergence, Q'_o, by calculating Q'_o as a residual in the mixed-layer energy budget as follows:

$$Q'_o = C_o \frac{\partial T'}{\partial t} - Q'_s \tag{1}$$

where T' is the monthly sea-surface temperature anomaly (assumed to be equal to the mixed-layer temperature anomaly) and Q'_s is the monthly surface heat flux anomaly. Note that the temperature tendency anomaly $\frac{\partial T'}{\partial t}$ is estimated using a centered finite difference with $\Delta t = 1$ month. The ocean mixed-layer heat capacity is given by $C_o = \rho c_p \overline{h}$, where $\overline{h}$ is the annual mean mixed-layer depth (MLD). Throughout most of the study, we use an annual-mean MLD from the ECCO ocean state estimate (Fig. 2b), which provides output from an ocean GCM (MITgcm) constrained to ocean observations between 1992-2015. We also highlight the sensitivity of select results to MLD from the ocean reanalysis ORAS5 (Zuo et al. 2019) at 0.25° horizontal resolution, and observed estimates from the French Research Institute for Exploitation of the Sea (IFREMER) at 2° horizontal resolution. Note that the IFREMER product combines a variety of in-situ density profiles, such as from Argo floats and the World Ocean Database (WOD09), that are also used in the ECCO product. In general, the spatial pattern of the annual-mean MLD agrees well across these products, however ECCO appears to overestimate the mean MLD in some regions, particularly in the Southern oceans as well as in the North Atlantic (Fig. 2b,c,d). Importantly, these discrepancies do not significantly impact the key results of this study as shown in Section 3.

The seasonality of the MLD also plays an important role in the variability of midlatitude SSTs (e.g. Deser et al. 2003). Thus, we also discuss the sensitivity of select results to seasonally-varying

Accepted for publication in *Journal of Climate*. DOI 10.1175/JCLI-D-21-0184.1.

MLD rather than annual-mean MLD. The use of a time-invariant MLD provides consistency with our formulation of the stochastic climate model and does not appear to influence the key results as shown in Section 3. Note that indirect estimates of ocean heat flux convergence derived using (1) may be biased due biases in the SST and/or surface heat flux data (e.g. Hall and Bryden 1982; Talley 1984; Bryden and Imawaki 2001). As such, estimates of the error in the SSTs and air-sea heat flux that are provided in the OAFlux product have been included in select figures throughout the paper.

We also analyze SSTs from slab-ocean model and fully-coupled configurations of CESM1 (Hurrell et al. 2013) under pre-industrial radiative forcing conditions at approximately 1° horizontal resolution. The model output was acquired from multi-century control runs provided in the CESM Large Ensemble Project (Kay et al. 2015). We have only analyzed the last $\sim$ 500 years of output to avoid potential issues with model spin-up. Both the slab-ocean and fully-coupled runs use the Community Atmosphere Model, version 5 (CAM5), but only the fully-coupled run includes an ocean GCM (POP2). In the case of the slab-ocean model (SOM), the atmospheric model is coupled to a spatially-varying but annual-repeating mixed layer depth (i.e., an annual-mean mixed-layer depth is prescribed from a fully-coupled run). The SOM has no ocean heat transport and is thus forced with a climatological-mean “q-flux" in order to maintain a realistic climate. The q-flux is constructed from a 20-year climatology of SSTs, mixed-layer depths, and surface heat fluxes from a fully-coupled control run (Bitz et al. 2012). Note that variations in SSTs are driven entirely by the surface heat fluxes in the SOM, but by both the surface heat fluxes and ocean dynamical processes in the fully-coupled model.

Accepted for publication in *Journal of Climate*. DOI 10.1175/JCLI-D-21-0184.1.

b. The simple stochastic climate model

In this section, we review the two configurations of the simple model that we use to probe the role of ocean processes in midlatitude SST variability. The simplest configuration is driven by the surface heat fluxes only, as illustrated by the black terms in Figure 1. We refer to this configuration of the model as the "heat flux model" throughout the study. The associated equation is as follows:

$$C_o \frac{\partial T'}{\partial t} = F_a - \lambda_s T' \tag{2}$$

Here, F_a is the forcing of SSTs by the surface heat fluxes associated with stochastic atmospheric dynamics, and $-\lambda_s T'$ is the damping of SSTs by the surface heat flux feedback. As previously discussed, in most cases we use an annual-mean MLD from ECCO (Fig. 2b) to calculate the mixed-layer heat capacity, C_o, which is consistent with previous formulations of stochastic climate models that use a time-invariant mixed layer depth.

In the more complex configuration, the heat flux model is extended to include two additional terms: forcing and damping by ocean processes (red terms in Fig. 1). We refer to this configuration of the model as the "ocean process model" throughout the study. Ocean processes that act to force SST anomalies have been included in simple models of midlatitude SST variability as 'ocean weather' (e.g. Wu et al. 2006; Smirnov et al. 2014; Bishop et al. 2017; Cane et al. 2017), advection by the wind-driven gyres (e.g. Czaja and Marshall 2000; Marshall et al. 2001; Qiu et al. 2007) and Ekman transport (e.g. Marshall et al. 2001). Ocean processes that act to damp temperature anomalies, such as vertical entrainment, have also been discussed in previous studies that used stochastic climate models (e.g. Frankignoul and Reynolds 1983; Frankignoul 1985; Frankignoul et al. 1998; Alexander and Penland 1996; Hall and Manabe 1997). However, to our knowledge, such a model has not been used to quantify the relative effects of oceanic forcing and oceanic damping processes on the frequency-dependent behavior of the observed SSTs.

Accepted for publication in *Journal of Climate*. DOI 10.1175/JCLI-D-21-0184.1.

The equation for the ocean process model used here is as follows:

$$C_o \frac{\partial T'}{\partial t} = F_a + F_o - \lambda T' \tag{3}$$

where

$$\lambda = \lambda_s + \lambda_o \tag{4}$$

Here, F_o and $-\lambda_o T'$ represent the oceanic forcing and damping terms, respectively, and hence $\lambda T'$ represents the total damping by both the surface heat fluxes and ocean processes. Note that equation (3) is equivalent to the heat flux model when the oceanic forcing and oceanic damping terms are set to zero, i.e., $F_o = 0$ and $\lambda_o = 0$.

The oceanic damping term, $-\lambda_o T'$, accounts primarily for the damping of mixed-layer temperatures by vertical entrainment (e.g. Frankignoul 1985; Hall and Manabe 1997; Frankignoul et al. 2002b; Mignot and Frankignoul 2003; Zhang 2017; Patrizio and Thompson 2021) but also mean advection in regions of strong ocean currents (Frankignoul and Reynolds 1983; Mignot and Frankignoul 2003). The role of ocean processes in damping SST variability has not been as widely explored as the role of ocean processes in forcing SST variability. Nevertheless, some studies have suggested that damping by ocean processes has comparable amplitude to damping by the surface heat fluxes (e.g. Frankignoul 1985; Hall and Manabe 1997; Mignot and Frankignoul 2003; Zhang 2017). Results from Patrizio and Thompson (2021) also suggest that vertical mixing plays a critical role in damping low-frequency SST variability throughout the Northern oceans.

The oceanic forcing term, F_o, can be considered the oceanic counterpart to the atmospheric forcing term, F_a, i.e., the forcing of SSTs by ocean dynamics. In other words, F_o accounts for ocean dynamical processes that act to drive SST variability in the ocean mixed-layer, including heat transport by ocean eddies. We do not make any *a priori* assumptions about either the oceanic forcing

Accepted for publication in *Journal of Climate*. DOI 10.1175/JCLI-D-21-0184.1.

term, F_o, or atmospheric forcing term, F_a, because both terms are estimated from observations as discussed in the following subsection.

c. Estimating the forcing and damping terms

The forcing (F_a, F_o) and damping (λ_s, λ_o) terms are estimated from observations following the method of Frankignoul and Kestenare (2002a; hereafter FK02; see also Park et al. 2005; Hausmann et al. 2016; Myers and Mechoso 2020). In this case the surface heat flux anomalies (Q'_s) are decomposed into a forcing term, Q^*_s, and a feedback term, $\lambda_s T'$, as follows:

$$Q'_s = Q^*_s - \lambda_s T' \tag{5}$$

where primes denote departures from the seasonal cycle. The surface heat flux damping coefficient, λ_s, is estimated using the following formula:

$$\lambda_s = -\frac{\overline{Q'_s T'_{-1}}}{\overline{T' T'_{-1}}} \tag{6}$$

Here, T'_{-1} denotes the SST anomalies leading the heat fluxes by one month. The surface heat flux damping is thus defined as the component of Q'_s that is linearly related to T' at a lag of one month (i.e., Q'_s lags T'), and the forcing term Q^*_s is defined as the residual. This definition assumes that the correlation between T' and the surface heat flux forcing Q^*_s approaches zero at a time lag of one month (this can be shown by multiplying both sides of Equation 5 by T'_{-1} and solving for λ_s). In other words, it assumes that the persistence of the atmospheric forcing is less than about one month. As discussed in FK02, if the atmospheric forcing persistence exceeds the time resolution of the lag used to compute λ_a, Q^*_s will be positively correlated with T' when Q^*_s lags T', and this will lead to a negative bias in the surface heat flux damping. In order to reduce this potential bias, we linearly remove variations in ENSO variability from the SST and surface heat flux anomalies before computing the damping and forcing terms. To remove ENSO, we linearly

Accepted for publication in *Journal of Climate*. DOI 10.1175/JCLI-D-21-0184.1.

regress contemporaneous values of the Niño 3.4 index from the fields. We use a single regression coefficient for all months. Similar results are derived when the regression coefficients vary as a function of month (not shown). In practice some persistence remains in the forcing terms even after removing the remote impact of ENSO variability, but this does not impact the key results as discussed in Section 3. Finally, note that FK02 computed the damping coefficient using equation (6) averaged over lead-times between 1 and 3 months instead of simply at a lead-time of 1 month, but we find little difference in the results in either case.

The FK02 method is likewise applied to the ocean heat flux convergence anomalies (Q'_o) to estimate the oceanic forcing term, F_o, and the oceanic damping coefficient, λ_o, as follows:

$$Q'_o = Q^*_o - \lambda_o T' \tag{7}$$

where

$$\lambda_o = -\frac{\overline{Q'_o T'_{-1}}}{\overline{T' T'_{-1}}} \tag{8}$$

As in the surface heat flux decomposition, Q^*_o is the ocean heat flux forcing, λ_o is the ocean heat flux damping coefficient, and the Niño 3.4 index is linearly regressed from the SST and ocean heat flux convergence anomalies prior to computing the damping and forcing terms. Thus, in the formulation of the ocean process model (eq. 3), we set $F_a = Q^*_s$ and the surface heat flux damping is set to λ_s, as calculated from (5) and (6), respectively. Likewise, we set $F_o = Q^*_o$ and the oceanic damping is set to λ_o, as calculated from (7) and (8), respectively.

To justify the similar treatment of Q'_s and Q'_o, Figure 3 shows the lag-correlations between Q'_o and T' (blue), and Q'_s and T' (green), averaged over two midlatitude regions in the North Pacific and North Atlantic (depicted by the boxes in Fig. 2a). Consistent with previous studies, Q'_s is positively correlated with the SST field at negative lags, which indicates forcing of the SST anomalies, and negatively correlated with the SST field at positive lags, which indicates damping

Accepted for publication in *Journal of Climate*. DOI 10.1175/JCLI-D-21-0184.1.

of the SST anomalies (e.g. Cayan 1992a,b; Frankignoul et al. 1998; von Storch 2000; Frankignoul and Kestenare 2002a; Bishop et al. 2017). Notably, the lag-correlations between Q'_o and the SSTs have a very similar structure, suggesting that SST anomalies are driven and damped by Q'_o in a similar manner. Some previous studies have argued that the asymmetric correlation between Q_s and the SSTs is suggestive of atmospheric-driven SSTs (e.g. Wu et al. 2006; O'Reilly et al. 2016; Bishop et al. 2017). However, the results shown in Fig. 3 suggest that this correlation structure does not preclude important contributions from ocean processes.

We focus primarily on the Northern midlatitude regions discussed previously mainly because they feature prominent SST variance (Fig. 2a), but it is important to note that the FK02 method appears to be applicable to both Q'_s and Q'_o throughout the midlatitudes, including the Southern oceans. In particular, the structure of the lag-correlations between the heat fluxes and the SSTs in most midlatitude regions is similar to that shown in Figure 3, albeit with weaker forcing from the surface heat fluxes in the western boundary current regions. On the other hand, the FK02 method does not appear suitable in tropical regions where lag-correlations generally remain positive at positive lags. This is indicative of greater persistence in the atmospheric and oceanic fields, which violates the key assumption of the FK02 method of estimating the forcing and damping terms. Indeed, as later shown in Fig. 8h, large errors are produced in the modeled SST variability at latitudes equatorward of about $\pm 20^{\circ}$.

To provide some physical insight into the oceanic damping term, $\lambda_o T'$, note that the vertical entrainment of heat between the deeper ocean and the mixed-layer can be expressed as proportional to $w_{ent}\,(T_b - T)$, where w_{ent} is the vertical entrainment rate and T_b is the temperature below the mixed-layer (e.g., Deser et al. 2010). Note here that we define the vertical entrainment rate to include all turbulent processes that add mass to the mixed-layer, and hence the entrainment is associated with a net upward mass flux (i.e., $w_{ent} > 0$). Decomposing the terms into a climatological mean

Accepted for publication in *Journal of Climate*. DOI 10.1175/JCLI-D-21-0184.1.

and a monthly-mean anomaly yields the following: $w_{ent}\left(T_b - T\right) \sim -w'_{ent}\overline{T} - \overline{w}_{ent}T'$, where we have neglected higher order terms and assumed that $T' >> T'_b$. Note that the first term, $-w'_{ent}\overline{T}$, can act to either force or damp SST anomalies depending on the sign of w'_{ent}. However, the second term, $-\overline{w}_{ent}T'$, always acts to *damp* SST anomalies because $\overline{w}_{ent} > 0$ by definition. Thus, the oceanic damping term, $\lambda_o T'$, includes the damping that arises from the mean vertical entrainment acting on SST anomalies. Note that the above reasoning is also relevant to the surface heat flux damping, except in this case the temperature difference is between the SST and the overlying air temperature, and the damping occurs via radiative processes as well as turbulent mixing.

We also note that the oceanic forcing term F_o accounts for all ocean dynamical processes that drive SST variability in the mixed-layer, including the horizontal advection of heat due by both mesoscale eddies and the wind-driven currents. Some previous studies interpret the wind-driven Ekman transport as an atmospheric forcing rather than oceanic forcing (e.g. Frankignoul and Reynolds 1983; Deser et al. 2010) since this transport is driven directly by the surface winds. However, here the wind-driven Ekman transport is retained in F_o in order to maintain physical consistency with other processes that transport heat in the ocean mixed-layer. Nevertheless, as discussed in section 3, F_o is generally dominated by non-Ekman transport throughout the midlatitudes, and hence our conclusions are not sensitive to whether the Ekman transport is included in F_o or F_a. Note also that—while vertical mixing can act to damp SST variability— F_o implicitly includes the variations in mixed-layer depth that act to force SST anomalies such as the reemergence mechanism (e.g. Alexander and Penland 1996; Deser et al. 2003; De Coëtlogon and Frankignoul 2003).

Accepted for publication in *Journal of Climate*. DOI 10.1175/JCLI-D-21-0184.1.

d. Power spectra

Analytical solutions to the power spectrum of the simple stochastic climate model are found as follows. First, equation (3) is transformed to frequency-space as:

$$T' = |T'|e^{2\pi i\omega t} \tag{9}$$

where ω is the frequency and t is the time. Equation (9) is then inserted into (3), yielding:

$$(C_o 2\pi i\omega - \lambda)T' = F_a + F_o \tag{10}$$

Taking the squared-magnitude of both sides (10) then yields:

$$|T'|^2 = \frac{|F_a|^2 + |F_o|^2}{\lambda^2 + 4\pi^2 C_o^2 \omega^2} \tag{11}$$

where we have made the assumption that the forcing terms are independent of each other, i.e., $|F_a F_o| = 0$. The assumption is predicated on our interpretation of F_a and F_o operating independently of each other. In principle, ocean dynamical processes are at least partially driven by atmospheric processes. But in practice, the covariance between F_a and F_o is negligible in the regions considered here.

3. Results

The results are presented in three subsections. In Section 3a, we show the observed estimates of the atmospheric and oceanic forcing and damping terms. In Section 3b, we exploit the two configurations of the simple stochastic climate model (i.e, the heat flux model and ocean process model) to explore the relative effects of the surface heat fluxes and ocean processes in driving midlatitude SST variability. In Section 3c, we test the reproducibility of the conclusions drawn from the simple model in output from slab-ocean and fully-coupled configurations of CESM.

Accepted for publication in *Journal of Climate*. DOI 10.1175/JCLI-D-21-0184.1.

a. Observed forcing and damping terms

Figures 4a,c show the variances of the atmospheric forcing (F_a) and oceanic forcing (F_o) terms, and Figures 4b,d show the surface heat flux damping (λ_s) and oceanic damping (λ_o) coefficients. All fields are derived from observations using the methodology described in Section 2. An annual-mean MLD from ECCO is used to compute the ocean terms unless indicated otherwise.

In general, the atmospheric forcing has the largest variance where the climatological-mean meridional SST gradients are strongest, such as in the vicinity of the Gulf Stream and Kuroshio currents. We suspect that is because regions of larger mean surface temperature gradients are associated with enhanced variability in the advective heat transport by the atmospheric flow (i.e., $u' \cdot \nabla\overline{T_a}$ is enhanced because $\nabla\overline{T_a}$ is larger), and thus in the forcing of SSTs via the surface heat fluxes. The variance of the oceanic forcing term exhibits a similar pattern, but with even more pronounced variance in regions with high ocean-eddy activity, including, for example, the Antarctic circumpolar current (ACC), and other regions where ocean dynamics are considered more active such as around the North Atlantic subpolar gyre (e.g. Buckley et al. 2014; Delworth et al. 2017; Zhang et al. 2019). Notably, the variance of the oceanic forcing term exceeds the variance of the atmospheric forcing term in many midlatitude regions. Note that the pattern and magnitude of the variances are largely identical when horizontal Ekman transport— as estimated using surface wind-stress from MERRA2 reanalysis— is included in F_a rather than F_o (not shown). This suggests that the oceanic forcing term is dominated by ocean dynamical processes other than horizontal Ekman transport.

The pattern of the surface heat flux damping coefficient (λ_s; Fig. 4b) is consistent with previous studies (e.g Frankignoul and Kestenare 2002a; Park et al. 2005; Hausmann et al. 2016). In particular, the surface heat flux damping coefficient is generally largest in the western parts of

Accepted for publication in *Journal of Climate*. DOI 10.1175/JCLI-D-21-0184.1.

the Northern Hemisphere ocean basins, consistent with the large air-sea humidity and temperature gradients in these regions. The surface heat flux damping coefficient is quite weak in some Northern high latitude regions, which appears to be due to the effects of sea-ice. That is, since the OAFlux product only provides data for ice-free points, high latitude regions are effectively masked when sea-ice forms during the winter, and thus the surface heat flux damping coefficient is dominated by the relatively weak damping that occurs during the warm season months (e.g Park et al. 2005).

The pattern of the oceanic damping coefficient (λ_o; Fig. 4d) closely resembles the pattern of the mean mixed-layer depth (Fig. 2b). That is, regions with stronger vertical mixing, such as the along the ACC or in the North Atlantic, are generally associated with stronger oceanic damping. An exception to this is in some regions along the Kuroshio current, where the mixed-layer is relatively deep, but our estimate of oceanic damping is relatively small. It is unclear whether this discrepancy reflects a bias in the methodology (see discussion in Section 2c), or biases in the mixed-layer depth in the Kuroshio region (compare Fig. 2b with Fig. 2d). Regardless, the discrepancy in this region does not change the broad conclusions supported by Figs. 4c,d, namely that the damping by ocean processes exceeds the damping by surface heat fluxes over vast regions of the midlatitudes. Finally, we note that the spatial patterns and magnitudes of the oceanic forcing and damping terms are similar when using seasonally-varying MLDs from ECCO to estimate the ocean heat flux convergence, rather than annual-mean MLDs (not shown). When using seasonally-varying MLDs, the oceanic forcing and damping are somewhat weaker throughout the midlatitudes with the largest discrepancies arising in the North Atlantic (when averaged across all midlatitudes, the oceanic forcing is about 10% weaker, and the oceanic damping is about 25% weaker). However, these discrepancies do not have any substantial impacts on the key results shown in the following subsection.

Accepted for publication in *Journal of Climate*. DOI 10.1175/JCLI-D-21-0184.1.

Figure 5 shows the spectral properties of F_a and F_o for the midlatitude North Atlantic (Fig. 5a) and midlatitude North Pacific (Fig. 5b) regions (depicted by the boxes in Figure 2a). The variance of the oceanic forcing term (blue) exceeds that of the atmospheric forcing term (green) at almost all resolved timescales in both midlatitude regions. This is particularly true in the midlatitude North Atlantic region, where the oceanic forcing variance is roughly an order of magnitude greater than the atmospheric forcing variance. We note that the differences between the variances of the atmospheric and oceanic forcing exceed the range of uncertainty provided by the OAFlux product, which has been plotted as transparent shading in Figure 5. We also note that oceanic forcing variance generally exceeds atmospheric forcing variance for all MLD products considered in this study (i.e., ECCO, ORAS5 and IFREMER), but their ratio decreases when using MLD from ORAS5 and IFREMER. For example, the ratio of oceanic forcing variance to atmospheric forcing variance in the midlatitude North Atlantic region is $\sim$5 for ECCO ~ 2.5 for ORAS5 and $\sim$1.5 for IFREMER. However, as later shown, these discrepancies do not affect the main conclusions of this study.

Figure 5 additionally indicates that the atmospheric forcing term can be roughly approximated by white-noise (darker green line), whereas the oceanic forcing term is better approximated as red-noise (darker blue line). The red-noise fit is computed by first producing a white-noise time series with total variance equal to the variance of $Q_o^*(t)$, and then reddening the resulting time series with lag-one autocorrelation given by $Q_o^*(t)$. This supports existing evidence that ocean dynamical processes are generally redder than their atmospheric counterparts (e.g Bjerknes 1964; Gulev et al. 2013).

Recall that the main assumption of the FK02 method used to estimate the forcing and damping terms is that the month-to-month persistence of the forcing terms is close to zero. In other words, the method assumes that the forcing terms can be approximated by white-noise on timescales greater

Accepted for publication in *Journal of Climate*. DOI 10.1175/JCLI-D-21-0184.1.

than about a month. As shown in Figure 5, this appears to be a valid assumption for the surface heat fluxes, but less so for the ocean heat flux convergence anomalies. We note, however, that the oceanic forcing spectra are essentially white on timescales longer than 0.5 years. Hence the oceanic forcing is only slightly more persistent than the atmospheric forcing term, and much less persistent than the SSTs (grey lines in Fig. 5). For example, the lag-1 autocorrelation averaged over the midlatitude North Atlantic region is $\sim$0.14 for the atmospheric forcing term, $\sim$0.25 for the oceanic forcing term and $\sim$0.73 for the SSTs. Regardless, the weak persistence in the oceanic forcing term suggests a violation of the main assumption inherent in the FK02 method and hence suggests that the oceanic damping term may be biased (as discussed in Section 2c). Thus, to quantify the range of possible biases in the damping terms, we performed an experiment wherein the simple model damping and forcing terms are prescribed and then the damping term is estimated using the FK02 method (see the Appendix for a more detailed discussion of the experiment). Importantly, we find that the weak autocorrelation in the forcing terms only lead to a small *underestimate* in the damping terms (Figure A1). Averaged across the midlatitudes, our analysis suggests that the oceanic damping term is only underestimated by about 10% and the surface heat flux damping term is only underestimated by about 5% as a result of the persistence in the respective forcing terms.

The dominance of the oceanic forcing term across many timescales and over large midlatitude regions as illustrated by Fig. 5 is surprising, and at first glance appears inconsistent with results from previous studies (e.g. Frankignoul and Reynolds 1983; Frankignoul et al. 1998; Bishop et al. 2017; Patrizio and Thompson 2021). For example, Frankignoul (1985) showed that the variance of atmospheric forcing generally dominates over the variance of oceanic forcing in the midlatitudes. This apparent discrepancy could be explained by their use of relatively low-resolution observational data (5°), which effectively neglected ocean eddy contributions (see also Frankignoul 1981 for more

Accepted for publication in *Journal of Climate*. DOI 10.1175/JCLI-D-21-0184.1.

discussion). In contrast, here we use higher-resolution observational data (1°) and hence suspect that a large fraction of the variance of the oceanic forcing term arises from relatively small-scale ocean eddies. In this regard, Bishop et al. (2017) also used higher-resolution observations to identify a surface heat flux signature of atmospheric-forced SSTs (i.e. an asymmetric correlation between Q_s and T) in the broad regions analyzed here. However, as discussed in Section 2c and suggested by Figs. 3 and 5, this surface heat flux signature of atmospheric-forced SSTs does not necessarily imply that oceanic forcing of SSTs is negligible. Finally, the results shown in Figure 5 also appear to contradict the findings in our companion paper (PT21), i.e., that ocean processes play a small role in driving low-frequency variability in midlatitude SSTs. However, as will become clear in the following subsection, the large effect of oceanic forcing indicated in Fig. 5 is generally overwhelmed by the pronounced effect of oceanic damping at low-frequencies.

b. Using the simple stochastic climate model to interpret the role of oceanic forcing and damping in SST variability

In this section, we use the two configurations of the simple stochastic climate model described in Section 2b to estimate the role of oceanic forcing and damping in SST variability. As shown in Table 1, we use the notation "H" to refer to the heat flux model solution (i.e., without oceanic forcing F_o and damping λ_o) and "H_{λ_o,F_o}" to refer to the ocean process model solution (i.e. with F_o and λ_o). Figure 6 illustrates the SST power spectra for H (green), H_{λ_o,F_o} (black), and the observed SST power spectra (grey), averaged over the two midlatitude Northern ocean regions depicted by the boxes in Figure 2a. Spectra are first calculated at individual grid points and then averaged over the domains. The forcing and damping values found in these regions are generally representative of most midlatitude regions. Later, we explore how results vary across all midlatitude oceans.

Accepted for publication in *Journal of Climate*. DOI 10.1175/JCLI-D-21-0184.1.

Importantly, Figure 6 shows that the heat flux model produces midlatitude SST power spectra that are too *red* relative to the observed power spectra (compare the green and grey lines). That is, the modeled spectra have too much power spectra at low frequencies, but too little power at high frequencies. The inclusion of ocean processes (i.e., both oceanic forcing and damping) acts to increase the power of the SST power spectra at high frequencies, but decrease it at low frequencies, which leads to an overall whitening of the midlatitude SST spectra. As such, the agreement between H_{λ_o,F_o} and the observed power spectrum is very good, with the exception of frequencies higher than ~ 0.5 years. Also note that the differences between H_{λ_o,F_o} and H are significant as measured by the uncertainty estimates provided by the OAFlux product (transparent shading). The high level of agreement between the observed spectra and the H_{λ_o,F_o} model is mostly due to our indirect method of estimating the ocean heat flux convergence in the ocean mixed layer. However, recall that the covariance between the forcing terms has been neglected in the derivation of the model SST power spectra (Section 2d). The close correspondence between the black and grey spectra thus indicates that the covariance between forcing terms is small and is not essential for capturing the general shape of the midlatitude SST power spectra.

The results highlighted in Figure 6 are generally consistent with previous findings from PT21, who argued that ocean dynamics act to reduce the variance of SSTs at low-frequencies throughout the Northern oceans. The results here similarly indicate the critical importance of oceanic damping processes for low-frequency SST variability in the Northern midlatitudes. In fact, as shown below, the results reveal that 1) oceanic damping overwhelms oceanic forcing on timescales greater than about 2 years, even though 2) oceanic forcing is an important source of midlatitude SST variance across many timescales as suggested by Figure 5.

Figure 7 quantifies the relative effects of the oceanic forcing and oceanic damping terms in the ocean process model. Figures 7a,b, are reproduced from Figure 6 but show another solution of the

Accepted for publication in *Journal of Climate*. DOI 10.1175/JCLI-D-21-0184.1.

model that *includes* oceanic damping ($\lambda_o T'$) but *excludes* oceanic forcing (F_o) (orange lines). The effect of oceanic damping on the SST power spectra is thus given by the difference between the green line (H) and orange line (H_{λ_o}), and the effect of ocean *forcing* on the SST power spectra is given by the difference between the black line (H_{λ_o,F_o}) and orange line (H_{λ_o}). As evidenced in the figure, oceanic damping acts to reduce the low-frequency SST variability (blue arrow in Figures 7a,b), whereas oceanic forcing increases the SST variability across many timescales (red arrows in Figures 7a,b).

Figures 7c,d further quantify the relative effects of oceanic forcing and oceanic damping on the modeled SST variability. Here we show the log-ratio of the power spectra for different configurations of the simple model: the red lines show the log-ratio of the modeled SST spectra with both oceanic damping and oceanic forcing (H_{λ_o,F_o}) to the modeled SST spectra with oceanic damping only (H_{λ_o}), and the blue lines show the log-ratio of the modeled SST spectra with oceanic damping only (H_{λ_o}) to the modeled SST spectra without any ocean processes (H). Hence the red lines quantify the effects of oceanic forcing as depicted by the red arrows in Figures 7a,b, and the blue lines quantify the effect of oceanic damping as depicted by the blue arrows in Figure 7a,b. The *net* effect of both oceanic forcing and oceanic damping is thus given by the sum of the red and blue lines and is shown as the black line.

From Figure 7c,d it is clear that oceanic forcing (F_o) is an important source of variability in both regions across many timescales, increasing the modeled SST power by a factor of about $10^{0.5} \approx 3$ on timescales between 0.2 to 25 years. However, it is also clear that the effects of oceanic damping processes ($\lambda_o T'$) outweigh the effects of oceanic forcing on timescales longer than $\sim$ 2 years. Thus, the combined effects of oceanic forcing and damping increase the variability of the SST field on timescales $<$ 2 years, but decrease it on timescales $>$ 2 years. Figure 7c,d also show that the whitening effect of the combined oceanic forcing and damping terms is substantial. As the

Accepted for publication in *Journal of Climate*. DOI 10.1175/JCLI-D-21-0184.1.

maximum effect, together they act to enhance the high-frequency power by about a factor of 3, but decrease the low-frequency power by roughly the same amount. Finally, note that the effects of oceanic forcing and damping illustrated in Figure 7 are reproducible when the model is forced by the white and red-noise fits indicated in Fig. 5 (not shown).

We have also explored the sensitivity of the modeled SST spectra shown to the use of different MLD products (see Figure 8). Importantly, we find qualitatively similar results for MLD from ECCO, ORAS5 and IFREMER. However, the contribution to SST variability from the oceanic forcing term generally decreases when using MLD from ORAS5 and IFREMER. We suspect that this is because ECCO generally exhibits larger MLDs compared to the other two products, and hence is associated with larger variance in the oceanic forcing term.

The above results are shown only for the two Northern midlatitude regions depicted by the boxes in Figure 2a. Figure 9 considers the relative effects of oceanic forcing and damping on the modeled low-frequency SST variance throughout the midlatitudes. Figure 9a shows the observed 5-year low-pass filtered SST variance and Figures 9b,c,d show the corresponding modeled variances derived from the various configurations of the simple model. Figures 9,e,f,g show maps of the log-ratio of the variances for the various configurations of the model.

In general, the heat flux model yields low-frequency SST variances that are notably larger than the observations throughout much of the midlatitudes (compare Figs 9a,b), particularly in Northern high latitude regions where the surface heat flux damping is weak (Fig. 4). The inclusion of oceanic damping in the simple model (H_{λ_o}) acts to greatly reduce the SST variance across the midlatitudes (Fig. 9e). However, the resulting variances are much too low compared to the observations (Fig. 9c). The inclusion of both oceanic damping *and* oceanic forcing in the model (H_{λ_o,F_o}) acts to increase the SST variance relative to the oceanic damping case (Fig. 9f) and the modeled SST variances are much closer to the observations (compare Figs. 9a,d).

Accepted for publication in *Journal of Climate*. DOI 10.1175/JCLI-D-21-0184.1.

As quantified in Fig. 9h, the differences between the observed and modeled low-frequency SST variances are generally small throughout the midlatitudes when both oceanic forcing and oceanic damping are included in the model. We have also verified not only that the ocean process model captures the observed low-frequency SST variance, but also that the model captures the observed spectra at individual points with different ocean dynamics, for example, in the Gulf Stream current and in the interior of the North Atlantic subpolar gyre (Fig. 10).

Note that the net effects of both ocean processes— as obtained by summing Fig. 9e and Fig. 9f— is generally dominated by oceanic damping (Fig. 9g). Thus, in the sum, ocean processes reduce the modeled low-frequency SST variance throughout most of the midlatitude oceans. Notable exceptions are found in western boundary current regions of the NH and the Agulhas current, where oceanic forcing overwhelms oceanic damping at low frequencies. For example, the dominance of oceanic forcing in the Gulf stream region is illustrated by Fig. 10a, which shows that the heat flux model greatly underestimates the SST variance across many timescales. This is consistent with the well-established role of ocean dynamical processes, such as mesoscale ocean eddies, in driving SST variability in these western boundary current regions (e.g. Kwon et al. 2010; Smirnov et al. 2014). Finally, we note that the magnitude and pattern of the effects of ocean processes on the modeled SST variability as shown in Fig. 9g is similar when using either annual-mean or seasonally-varying MLDs from ECCO, ORAS5 or IFREMFER (not shown). The broad agreement across the various treatments of the MLD provides further evidence of the robustness our results.

c. Slab-ocean and fully-coupled simulations with CESM

In this section, we use the simple stochastic climate model to interpret the differences in SST variability between simulations run with an atmospheric model coupled to a slab-ocean model

Accepted for publication in *Journal of Climate*. DOI 10.1175/JCLI-D-21-0184.1.

(referred to as the SOM) and a dynamically-active ocean model (referred to as the fully-coupled model).

As discussed in Section 2a, we have analyzed 500 years of data from pre-industrial runs with CESM1 (Hurrell et al. 2013). Both are run with preindustrial forcing. The heat flux model is considered to be analogous to the slab-ocean configuration since neither include ocean dynamical processes, and likewise, the ocean process model is considered to be analogous to the fully-coupled configuration since both *do* include ocean dynamical processes: the ocean process model through the terms F_o and $-\lambda_o T'$, and the fully-coupled model through simulated ocean dynamical processes. Note that we have also verified that the spatial pattern and magnitudes of the surface heat flux damping and variance of the atmospheric forcing term are similar in both the SOM and fully-coupled run (not shown). Critically, this means that the differences in SST variability between the SOM and fully-coupled run can be attributed to ocean dynamical processes.

Figure 11 shows the 5-year low-pass filtered SST variance in the SOM (Fig. 11a) and the fully-coupled model (Fig. 11b), as well as the log-ratio of their variances (Fig. 11c). In the tropics, the low-frequency SST variance is larger in the fully-coupled model, which is expected given that ocean dynamics are known to play a prominent role in driving SST variability in these regions (e.g. Philander 1983; Jin 1997; McPhaden et al. 2006). However, in the extratropics, the low-frequency SST variance is generally *larger* in the SOM configuration. This seemingly surprising result is consistent with the results in the previous section, namely that ocean processes act to decrease the low-frequency variance of extratropical SSTs (e.g. Fig. 9g).

Figure 12 compares the SST power spectra averaged over the midlatitude North Atlantic and North Pacific regions computed from both the simple model (Figs. 13a,d) and the SOM and fully-coupled configurations of CESM (Figs. 13b,e). Note that all power spectra are first calculated at individual grid points and then averaged over the respective domains. Clearly, the models that

Accepted for publication in *Journal of Climate*. DOI 10.1175/JCLI-D-21-0184.1.

include ocean processes (black lines in Figs. 13a,b,d,e) have relatively less low-frequency SST variance but relatively more high-frequency variance than the models that do not include ocean dynamical processes (green lines in Figs. 13a,b,d,e). The similarities between spectra are striking, particularly in the midlatitude North Atlantic. This is also reflected in Figures 12c,f, which show the log-ratio of the modeled SST spectra with ocean processes to the modeled SST spectra without ocean processes for both the simple model (grey) and CESM (black). Here, it can be seen that the simple model captures the overall whitening effect of ocean dynamical processes in CESM (i.e., decrease in low-frequency variance but increase in high-frequency variance), particularly in the midlatitude North Atlantic (Fig. 13c). Note that qualitatively similar results to those shown in Fig. 13 are derived for midlatitude Southern ocean regions as well, particularly in the South Atlantic and South Indian oceans.

Up to this point the analyses have been performed at the grid-point level, i.e., the CESM and simple model spectra have been computed at the grid-point level and then averaged over large regions. Thus it is unclear whether our results also apply to basin-scale modes of SST variability, such as AMV or PDV. As discussed by Zhang (2017) larger-scale SST anomalies generally have weaker surface heat flux damping rates than SST anomalies estimated at individual grid points because larger-scale SST anomalies tend to interact very differently with the atmosphere than smaller-scale SST anomalies (e.g. Frankignoul 1985; Kleeman and Power 1995). Similar arguments could be made for oceanic damping rates, and so the possible differences in damping at large spatial-scales may also translate to differences in the modeled SST spectra. Thus, to test the robustness of the results to basin-scale SST variability, Figure 14 shows a reproduction of Figure 13 except that the CESM and simple model spectra have been computed for area-averaged SSTs. Notably, the whitening effect of ocean dynamics also acts on both North Atlantic and North Pacific averaged SST anomalies. This suggests that basin-scale modes of SST variability are also affected by the

Accepted for publication in *Journal of Climate*. DOI 10.1175/JCLI-D-21-0184.1.

damping effect of ocean dynamics at low-frequencies. Consistent with the discussions of Zhang (2017), we find that both the surface heat flux and oceanic damping parameters are weaker when evaluated for area-averaged SSTs rather than at the grid-point level. However, Fig. 14 suggests that this generally does not influence the conclusions of our study.

Figure 13 and Figure 14 also indicate two interesting differences between the simple model and CESM. First, in the midlatitude North Pacific, CESM does not show any reduction in low-frequency variance ($>$ 5 years) in the fully-coupled model relative to the SOM (Fig. 12f and Fig. 14f). This could be due to the presence of atmosphere-ocean interactions that are unique to the fully-coupled model, which might act to enhance low-frequency variance in the North Pacific (e.g. Qiu et al. 2007; Kwon and Deser 2007; Kwon et al. 2010; Wills et al. 2019a) and offset the effects of oceanic damping.

Zhang (2017) argued that such atmosphere-ocean interactions enhance the low-frequency variability of North Atlantic subpolar SSTs. In particular, it was found that SST variance on $\sim$15 to 100 year timescales in the subpolar North Atlantic was enhanced in a fully-coupled configuration of GFDL's GCM (CM2.1) compared to its slab-ocean configuration. However, in CESM this effect is not readily apparent (see Figs. 12c and Fig. 14c, and we have also verified that this is true up to 100 year timescales, which are not displayed in Figures 13 and 14). Interestingly, we note that GFDL's CM2.1 seemingly exhibits the whitening effect of ocean dynamics on timescales *less* than $\sim$15 years (see Figure 2b of Zhang 2017). The discrepancies between Zhang (2017) and our results at timescales greater than $\sim$15 years could derive from their use of a different GCM and/or their use of normalized power spectra.

The second key difference between the simple model and CESM spectra is that the crossover frequency at which the models with ocean processes have more variance than the models without ocean processes occurs at higher frequencies for CESM compared to the simple model (i.e., in

Accepted for publication in *Journal of Climate*. DOI 10.1175/JCLI-D-21-0184.1.

Figures 12c,f the curve for CESM is shifted to the right compared to the simple model). Our interpretation of this discrepancy is as follows: 1) oceanic forcing is likely unrealistically weak in CESM due to its relatively coarse 1° horizontal resolution, and 2) the unrealistically weak oceanic forcing means that the effects of oceanic damping will likely overwhelm the effects of oceanic forcing at higher-frequencies compared to the observationally-constrained simple model. According to our analyses, unrealistically weak oceanic forcing would manifest most clearly as reduced high-frequency SST variance. Indeed, we have found that the high-frequency SST variance (1-year high-pass filtered) is lower in CESM than in the observations throughout the midlatitudes (not shown), supporting the hypotheses above.

Despite these two discrepancies, the broad agreement between the low-frequency variances and SST spectra derived from the simple model and CESM (as shown in Figure 9g, Figure 11, Figure 12c, Figure 13 and Figure 14) support our primary hypothesis that the net impact of ocean dynamics is to decrease the low-frequency SST variance and increase the high-frequency SST variance throughout the midlatitudes.

4. Discussion and Conclusions

The goal of this study is to provide novel insights into the role of ocean dynamics in midlatitude SST variability using the stochastic climate model framework (Hasselmann 1976; Frankignoul and Hasselmann 1977). In particular, we have considered two different configurations of a simple stochastic climate model: one that is driven only by surface heat fluxes, and another that includes the forcing and damping of SST variability by ocean processes.

The key conclusion is that throughout most of the midlatitudes, the net effect of ocean processes is to increase the variance of SST anomalies at high-frequencies, but *decrease* the variance at low-frequencies. Specifically, we have found that:

Accepted for publication in *Journal of Climate*. DOI 10.1175/JCLI-D-21-0184.1.

1. The simple stochastic climate model driven by observed surface heat fluxes yields midlatitude SST power spectra that are much redder than observed midlatitude SST power spectra (Fig. 6).

2. Including observed estimates of both oceanic forcing and oceanic damping in the simple model reduces the discrepancy with the observations by decreasing the SST variance on timescales > 2 years and increasing the SST variance on timescales < 2 years, leading to an overall "whitening" of the midlatitude SST variability (Fig. 6). The whitening effect arises because oceanic forcing is an important source of SST variance across many timescales, but the effects of oceanic damping exceed the effects of oceanic forcing timescales $> \sim 2$ years (Fig. 7). Exceptions to this result were found to occur in regions of strong currents such as the Kuroshio, Gulf Stream and Agulhas currents, where the effects of oceanic forcing exceed the effects of oceanic damping (Fig. 9g and Fig. 10).

3. Model output from GCM simulations run on slab-ocean and dynamically-active ocean (i.e., fully-coupled) model configurations of CESM1 also indicates that ocean dynamical processes reduce the low-frequency variance and increase the high-frequency variance of the SST field in many midlatitude regions (Fig. 12, Fig. 13 and Fig. 14).

This study extends previous work that has also added ocean processes to simple stochastic climate models in two key ways:

- We have decomposed observed estimates of the ocean-mixed layer heat flux convergence— calculated as a residual in the mixed-layer energy budget using observation-based SSTs, surface heat fluxes and mixed-layer depths— into oceanic forcing and oceanic damping terms. This is in contrast to studies that have assumed the form of the oceanic forcing (e.g Wu et al. 2006; Cane et al. 2017; Bishop et al. 2017) or estimated the total damping from the

Accepted for publication in *Journal of Climate*. DOI 10.1175/JCLI-D-21-0184.1.

autocorrelation of SSTs (e.g. Frankignoul and Hasselmann 1977; Reynolds 1978; Frankignoul 1979; Hall and Manabe 1997).

- We use the simple model to quantify the relative roles of oceanic forcing and oceanic damping in observed SST variability. This is in contrast to studies that more generally comparing red-noise SST power spectra to observed SST power spectra (e.g Frankignoul and Hasselmann 1977; Reynolds 1978; Frankignoul 1979; Hall and Manabe 1997; Zhang 2017).

The results shown here provide insight into the processes that give rise to low-frequency SST variability in models with and without ocean dynamics (e.g. Clement et al. 2015; Cane et al. 2017; Zhang 2017; Murphy et al. 2021). For example, Cane et al. (2017) and Murphy et al. (2021) demonstrated that the simulated Atlantic Multidecadal Variability (AMV) in SSTs is reduced in a fully-coupled configuration of CESM relative to a slab-ocean configuration (see Figure 1 of Cane et al. 2017 and Figure 4 of Murphy et al. 2021). As evidenced in Figures 12 and 13, the differences in North Atlantic SST variability between the fully-coupled and slab-ocean (SOM) configurations of CESM are well-captured by the simple model. Thus, we can use the simple model to interpret the effects of ocean dynamics on North Atlantic SST variability in CESM, i.e., in CESM, oceanic forcing increases the variance of North Atlantic SSTs across many timescales, but oceanic damping outweighs oceanic forcing at low-frequencies. It would be interesting to use the insights provided by the simple stochastic climate model used here to better understand the differences between other SOM and fully-coupled GCMs, including models with higher spatial resolution.

Clement et al. (2015) argued that ocean dynamics are not essential for generating AMV. We have shown that slab-ocean models can not only generate AMV, but in fact generate too much low-frequency SST variance throughout the midlatitudes, at least in the case of CESM. However, our simple model also suggests that the processes that give rise to such low-frequency SST variability

Accepted for publication in *Journal of Climate*. DOI 10.1175/JCLI-D-21-0184.1.

in models with ocean dynamics are different. Without either oceanic damping *or* oceanic forcing in the simple model, the low-frequency SST variance is significantly different in terms of both spatial pattern and magnitude throughout the midlatitudes (Fig. 9). The broad agreement between the observationally-constrained simple model and CESM suggests that the oceanic forcing and oceanic damping are important for midlatitude SST variability in reality.

In our previous study (Patrizio and Thompson 2021), we argued that midlatitude ocean dynamics play an increasingly small role in driving SST variability at increasingly low-frequencies. The results presented here provide key insights into this hypothesis. In agreement with results from our previous study, the simple model and CESM results shown here suggest that the *net* effect of oceanic forcing and damping is to decrease the SST variance at low-frequencies, and increase it at high-frequencies throughout the midlatitudes. The simple model provides insights into how this happens. That is, it reveals that oceanic forcing does in fact act to redden the spectra of midlatitude SST anomalies (Fig. 5), but that this effect is generally overwhelmed by the effects of oceanic damping away from western boundary currents (Fig. 9g). This important result was not found in our previous study because there we diagnosed the *net* effect of ocean dynamics, whereas here we have used a simple stochastic climate model to diagnose the *individual* effects of ocean dynamical forcing and damping.

Hence the results of this study make clear that midlatitude ocean dynamics play an important role in driving low-frequency SST variability through the combined effects of both oceanic forcing and oceanic damping processes. The importance of oceanic forcing supports previous studies that have linked low-frequency variations in SSTs to ocean dynamical processes, such as the AMOC (e.g. Buckley et al. 2014; Kim et al. 2018; O'Reilly et al. 2016; Wills et al. 2019b,a; Zhang et al. 2019). However, the importance of oceanic damping also explains why previous studies have found that models without ocean processes (e.g., slab-ocean models) can generate low-frequency SST

Accepted for publication in *Journal of Climate*. DOI 10.1175/JCLI-D-21-0184.1.

variance that is comparable (or even exceeds) that in models with comprehensive ocean dynamics (e.g Clement et al. 2015; Cane et al. 2017; Murphy et al. 2021).

The results from our previous study (Patrizio and Thompson 2021) suggest that vertical mixing primarily accounts for the oceanic damping of low-frequency SST variability throughout much of the Northern oceans as inferred by the ocean state estimate ECCO. Supporting these results, Yamamoto et al. (2020) has also shown that mixed-layer deepening and vertical entrainment play critical roles in decadal variability of subpolar North Atlantic SSTs in MIROC6. However, further research is needed to better understand the detailed physics behind both the oceanic forcing and damping of midlatitude SST variability in both observations and GCMs.

Data availability statement. Observational and reanalysis data are freely accessible online: OAFlux (`http://oaflux.whoi.edu/`), ECCO (https://ecco.jpl.nasa.gov/), MERRA-2 reanalysis (`https://gmao.gsfc.nasa.gov/reanalysis/MERRA-2/`, ORAS5 reanalysis (`https://www.ecmwf.int/en/research/climate-reanalysis/ocean-reanalysis`), and observed MLD from IFREMER (`http://www.ifremer.fr/cerweb/deboyer/mld/Surface_Mixed_Layer_Depth.php`). CESM output is available on NCAR's supercomputing system and can be provided upon request.

Acknowledgments. CP was supported by the NASA Earth and Space Science Fellowship 80NSSC18K1345 and partially supported by the NSF Climate and Large-Scale Dynamics program. DWJT is supported by the NSF Climate and Large-Scale Dynamics program. We thank Laure Zanna, Claude Frankignoul, Cristian Proistosescu and two reviewers for their thoughtful and constructive comments on the manuscript.

APPENDIX

Accepted for publication in *Journal of Climate*. DOI 10.1175/JCLI-D-21-0184.1.

As discussed in Section 2c, persistence in the simple model forcing terms can result in biased estimates of the damping terms from Eqs. (7) and (8). Here, we describe the experiment used to quantify these biases. We start with a more general stochastic climate model (Hasselmann 1976) with stochastic forcing term F and linear damping parameter λ:

$$\rho c_p \overline{h} \frac{\partial T'}{\partial t} = F - \lambda T' \tag{A1}$$

The forcing term F is assumed to be red-noise with variable lag-1 autocorrelation (r_1) ranging from 0 to 0.9. The variance of F is set to 3000 W^2 K^4, the damping term is set to λ = 35 W m^{-2} K^{-1} and mixed-layer depth $\overline{h}$ = 100 m. To acquire the time evolution of T, equation (A1) is discretized at monthly resolution and integrated forward in time using a forward-difference method.

The total heat flux convergence anomalies Q' are then calculated by adding the prescribed forcing and damping terms (i.e. using Eq. 5 or 6) as follows:

$$Q' = F + \lambda T' \tag{A2}$$

where T' is the numerically integrated model solution from (A1). The damping is then estimated using the FK02 method (i.e. Eq. 7 or 8) as follows:

$$\lambda_e = -\frac{\overline{Q'T'_{-1}}}{\overline{T'T'_{-1}}} \tag{A3}$$

where T'_{-1} denotes the SST anomalies leading the heat fluxes by one month. The bias is then given by the difference between the prescribed damping $\lambda = 35$ W m^{-2} K^{-1}, and the FK02 estimate of the damping, λ_e, calculated from (A3).

Figure A1 shows λ_e for a range of r_1 values. Note that the experiment is performed 100 times for each r_1 value to sample the range of possible biases that would arise from internal variability in the forcing term. Consistent with the discussion in Section 2c, Figure A1 shows that increasing r_1 in the forcing term leads to a greater negative bias in estimated damping term. Importantly, however,

Accepted for publication in *Journal of Climate*. DOI 10.1175/JCLI-D-21-0184.1.

for the observed range of r_1 in the atmospheric and oceanic forcing terms (green and blue shading), the damping term is only slightly underestimated. When averaged across all midlatitudes, this leads to a $\sim$5% bias in the case of the surface heat flux damping and $\sim$10% bias in the oceanic damping. We have also verified that such biases are only associated with small changes in the modeled SST spectra and hence do not affect the main conclusions of this study.

References

Alexander, M., and Coauthors, 2010: Extratropical air–sea interaction, sea surface temperature variability, and the Pacific decadal oscillation. *Climate Dynamics: Why Does Climate Vary?, Geophys. Monogr*, **189**, 123–148.

Alexander, M. A., I. Bladé, M. Newman, J. R. Lanzante, N.-C. Lau, and J. D. Scott, 2002: The atmospheric bridge: The influence of ENSO teleconnections on air–sea interaction over the global oceans. *Journal of climate*, **15 (16)**, 2205–2231.

Alexander, M. A., and C. Penland, 1996: Variability in a mixed layer ocean model driven by stochastic atmospheric forcing. *Journal of Climate*, **9 (10)**, 2424–2442.

Barsugli, J. J., and D. S. Battisti, 1998: The basic effects of atmosphere–ocean thermal coupling on midlatitude variability. *Journal of the Atmospheric Sciences*, **55 (4)**, 477–493.

Bellomo, K., L. N. Murphy, M. A. Cane, A. C. Clement, and L. M. Polvani, 2018: Historical forcings as main drivers of the Atlantic multidecadal variability in the CESM large ensemble. *Climate Dynamics*, **50 (9-10)**, 3687–3698.

Bellucci, A., and Coauthors, 2020: Air-sea interaction over the gulf stream in an ensemble of HighResMIP present climate simulations. *Climate Dynamics*, 1–19.

Accepted for publication in *Journal of Climate*. DOI 10.1175/JCLI-D-21-0184.1.

Bishop, S. P., R. J. Small, F. O. Bryan, and R. A. Tomas, 2017: Scale dependence of midlatitude air–sea interaction. *Journal of Climate*, **30 (20)**, 8207–8221.

Bitz, C. M., K. Shell, P. Gent, D. Bailey, G. Danabasoglu, K. Armour, M. Holland, and J. Kiehl, 2012: Climate sensitivity of the community climate system model, version 4. *Journal of Climate*, **25 (9)**, 3053–3070.

Bjerknes, J., 1964: Atlantic air-sea interaction. *Advances in geophysics*, Vol. 10, Elsevier, 1–82.

Bryden, H. L., and S. Imawaki, 2001: Ocean heat transport. *International Geophysics*, Vol. 77, Elsevier, 455–474.

Buckley, M. W., and J. Marshall, 2016: Observations, inferences, and mechanisms of the Atlantic Meridional Overturning Circulation: A review. *Reviews of Geophysics*, **54 (1)**, 5–63.

Buckley, M. W., R. M. Ponte, G. Forget, and P. Heimbach, 2014: Low-frequency SST and upper-ocean heat content variability in the North Atlantic. *Journal of Climate*, **27 (13)**, 4996–5018.

Buckley, M. W., R. M. Ponte, G. Forget, and P. Heimbach, 2015: Determining the origins of advective heat transport convergence variability in the North Atlantic. *Journal of Climate*, **28 (10)**, 3943–3956.

Cane, M. A., A. C. Clement, L. N. Murphy, and K. Bellomo, 2017: Low-pass filtering, heat flux, and Atlantic multidecadal variability. *Journal of Climate*, **30 (18)**, 7529–7553.

Cayan, D. R., 1992a: Latent and sensible heat flux anomalies over the northern oceans: Driving the sea surface temperature. *Journal of Physical Oceanography*, **22 (8)**, 859–881.

Cayan, D. R., 1992b: Latent and sensible heat flux anomalies over the northern oceans: The connection to monthly atmospheric circulation. *Journal of climate*, **5 (4)**, 354–369.

Accepted for publication in *Journal of Climate*. DOI 10.1175/JCLI-D-21-0184.1.

Clement, A., K. Bellomo, L. N. Murphy, M. A. Cane, T. Mauritsen, G. Rädel, and B. Stevens, 2015: The Atlantic Multidecadal Oscillation without a role for ocean circulation. *Science*, **350 (6258)**, 320–324.

Czaja, A., and J. Marshall, 2000: On the interpretation of AGCMs response to prescribed time-varying SST anomalies. *Geophysical research letters*, **27 (13)**, 1927–1930.

De Coëtlogon, G., and C. Frankignoul, 2003: The persistence of winter sea surface temperature in the North Atlantic. *Journal of climate*, **16 (9)**, 1364–1377.

Delworth, T. L., F. Zeng, L. Zhang, R. Zhang, G. A. Vecchi, and X. Yang, 2017: The central role of ocean dynamics in connecting the North Atlantic Oscillation to the extratropical component of the Atlantic Multidecadal Oscillation. *Journal of Climate*, **30 (10)**, 3789–3805.

Deser, C., M. A. Alexander, and M. S. Timlin, 2003: Understanding the persistence of sea surface temperature anomalies in midlatitudes. *Journal of Climate*, **16 (1)**, 57–72.

Deser, C., M. A. Alexander, S.-P. Xie, and A. S. Phillips, 2010: Sea surface temperature variability: Patterns and mechanisms. *Annual review of marine science*, **2**, 115–143.

Deser, C., A. S. Phillips, and J. W. Hurrell, 2004: Pacific interdecadal climate variability: Linkages between the tropics and the North Pacific during boreal winter since 1900. *Journal of Climate*, **17 (16)**, 3109–3124.

Frankignoul, C., 1979: Stochastic forcing models of climate variability. *Dynamics of Atmospheres and Oceans*, **3 (2-4)**, 465–479.

Frankignoul, C., 1981: Low-frequency temperature fluctuations off Bermuda. *Journal of Geophysical Research: Oceans*, **86 (C7)**, 6522–6528.

Accepted for publication in *Journal of Climate*. DOI 10.1175/JCLI-D-21-0184.1.

Frankignoul, C., 1985: Sea surface temperature anomalies, planetary waves, and air-sea feedback in the middle latitudes. *Reviews of geophysics*, **23 (4)**, 357–390.

Frankignoul, C., A. Czaja, and B. L'Heveder, 1998: Air–sea feedback in the North Atlantic and surface boundary conditions for ocean models. *Journal of climate*, **11 (9)**, 2310–2324.

Frankignoul, C., and K. Hasselmann, 1977: Stochastic climate models, Part ii: Application to sea-surface temperature anomalies and thermocline variability. *Tellus*, **29 (4)**, 289–305.

Frankignoul, C., and E. Kestenare, 2002a: The surface heat flux feedback. Part i: Estimates from observations in the Atlantic and the North Pacific. *Climate dynamics*, **19 (8)**, 633–647.

Frankignoul, C., E. Kestenare, and J. Mignot, 2002b: The surface heat flux feedback. Part II: direct and indirect estimates in the ECHAM4/OPA8 coupled GCM. *Climate dynamics*, **19 (8)**, 649–655.

Frankignoul, C., and R. W. Reynolds, 1983: Testing a dynamical model for mid-latitude sea surface temperature anomalies. *Journal of physical oceanography*, **13 (7)**, 1131–1145.

Frenger, I., N. Gruber, R. Knutti, and M. Münnich, 2013: Imprint of Southern Ocean eddies on winds, clouds and rainfall. *Nature geoscience*, **6 (8)**, 608–612.

Gelaro, R., and Coauthors, 2017: The modern-era retrospective analysis for research and applications, version 2 (MERRA-2). *Journal of Climate*, **30 (14)**, 5419–5454.

Gulev, S. K., M. Latif, N. Keenlyside, W. Park, and K. P. Koltermann, 2013: North Atlantic Ocean control on surface heat flux on multidecadal timescales. *Nature*, **499 (7459)**, 464–467.

Hall, A., and S. Manabe, 1997: Can local linear stochastic theory explain sea surface temperature and salinity variability? *Climate Dynamics*, **13 (3)**, 167–180.

Accepted for publication in *Journal of Climate*. DOI 10.1175/JCLI-D-21-0184.1.

Hall, M. M., and H. L. Bryden, 1982: Direct estimates and mechanisms of ocean heat transport. *Deep Sea Research Part A. Oceanographic Research Papers*, **29 (3)**, 339–359.

Hasselmann, K., 1976: Stochastic climate models part I. Theory. *tellus*, **28 (6)**, 473–485.

Hausmann, U., A. Czaja, and J. Marshall, 2016: Estimates of air–sea feedbacks on sea surface temperature anomalies in the southern ocean. *Journal of Climate*, **29 (2)**, 439–454.

Hurrell, J. W., and Coauthors, 2013: The community earth system model: a framework for collaborative research. *Bulletin of the American Meteorological Society*, **94 (9)**, 1339–1360.

Jin, F.-F., 1997: An equatorial ocean recharge paradigm for ENSO. Part i: Conceptual model. *Journal of the atmospheric sciences*, **54 (7)**, 811–829.

Kay, J. E., and Coauthors, 2015: The community earth system model (CESM) large ensemble project: A community resource for studying climate change in the presence of internal climate variability. *Bulletin of the American Meteorological Society*, **96 (8)**, 1333–1349.

Kim, W. M., S. G. Yeager, and G. Danabasoglu, 2018: Key role of internal ocean dynamics in atlantic multidecadal variability during the last half century. *Geophysical Research Letters*, **45 (24)**, 13–449.

Kirtman, B. P., and Coauthors, 2012: Impact of ocean model resolution on CCSM climate simulations. *Climate dynamics*, **39 (6)**, 1303–1328.

Kleeman, R., and S. B. Power, 1995: A simple atmospheric model of surface heat flux for use in ocean modeling studies. *Journal of physical oceanography*, **25 (1)**, 92–105.

Kwon, Y.-O., M. A. Alexander, N. A. Bond, C. Frankignoul, H. Nakamura, B. Qiu, and L. A. Thompson, 2010: Role of the Gulf Stream and Kuroshio–Oyashio systems in large-scale atmosphere–ocean interaction: A review. *Journal of Climate*, **23 (12)**, 3249–3281.

Accepted for publication in *Journal of Climate*. DOI 10.1175/JCLI-D-21-0184.1.

Kwon, Y.-O., and C. Deser, 2007: North Pacific decadal variability in the community climate system model version 2. *Journal of climate*, **20 (11)**, 2416–2433.

Ma, X., and Coauthors, 2015: Distant influence of Kuroshio eddies on North Pacific weather patterns? *Scientific reports*, **5**, 17 785.

Ma, X., and Coauthors, 2016: Western boundary currents regulated by interaction between ocean eddies and the atmosphere. *Nature*, **535 (7613)**, 533–537.

Marshall, J., H. Johnson, and J. Goodman, 2001: A study of the interaction of the North Atlantic Oscillation with ocean circulation. *Journal of Climate*, **14 (7)**, 1399–1421.

McPhaden, M. J., S. E. Zebiak, and M. H. Glantz, 2006: ENSO as an integrating concept in earth science. *science*, **314 (5806)**, 1740–1745.

Mignot, J., and C. Frankignoul, 2003: On the interannual variability of surface salinity in the atlantic. *Climate dynamics*, **20 (6)**, 555–565.

Murphy, L. N., K. Bellomo, M. A. Cane, and A. C. Clement, 2017: The role of historical forcings in simulating the observed Atlantic multidecadal oscillation. *Geophysical Research Letters*, **44 (5)**, 2472–2480.

Murphy, L. N., J. M. Klavans, A. C. Clement, and M. A. Cane, 2021: Investigating the roles of external forcing and ocean circulation on the atlantic multidecadal sst variability in a large ensemble climate model hierarchy. *Journal of Climate*, **34 (12)**, 4835–4849.

Myers, T. A., and C. R. Mechoso, 2020: Relative contributions of atmospheric, oceanic, and coupled processes to north pacific and north atlantic variability. *Geophysical Research Letters*, **47 (5)**, e2019GL086 321.

Accepted for publication in *Journal of Climate*. DOI 10.1175/JCLI-D-21-0184.1.

Newman, M., G. P. Compo, and M. A. Alexander, 2003: ENSO-forced variability of the Pacific decadal oscillation. *Journal of Climate*, **16 (23)**, 3853–3857.

Newman, M., and Coauthors, 2016: The Pacific decadal oscillation, revisited. *Journal of Climate*, **29 (12)**, 4399–4427.

O'Reilly, C. H., M. Huber, T. Woollings, and L. Zanna, 2016: The signature of low-frequency oceanic forcing in the Atlantic Multidecadal Oscillation. *Geophysical Research Letters*, **43 (6)**, 2810–2818.

Park, S., C. Deser, and M. A. Alexander, 2005: Estimation of the surface heat flux response to sea surface temperature anomalies over the global oceans. *Journal of climate*, **18 (21)**, 4582–4599.

Patrizio, C. R., and D. W. Thompson, 2021: Quantifying the Role of Ocean Dynamics in Ocean Mixed-Layer Temperature Variability. *Journal of Climate*, 1–63.

Philander, S. G. H., 1983: El-niño southern oscillation phenomena. *Nature*, **302 (5906)**, 295–301.

Putrasahan, D., I. Kamenkovich, M. Le Hénaff, and B. Kirtman, 2017: Importance of ocean mesoscale variability for air-sea interactions in the Gulf of Mexico. *Geophysical Research Letters*, **44 (12)**, 6352–6362.

Qiu, B., N. Schneider, and S. Chen, 2007: Coupled decadal variability in the North Pacific: An observationally constrained idealized model. *Journal of Climate*, **20 (14)**, 3602–3620.

Reynolds, R. W., 1978: Sea surface temperature anomalies in the North Pacific Ocean. *Tellus*, **30 (2)**, 97–103.

Reynolds, R. W., T. M. Smith, C. Liu, D. B. Chelton, K. S. Casey, and M. G. Schlax, 2007: Daily high-resolution-blended analyses for sea surface temperature. *Journal of Climate*, **20 (22)**, 5473–5496.

Accepted for publication in *Journal of Climate*. DOI 10.1175/JCLI-D-21-0184.1.

Roberts, C. D., M. D. Palmer, R. P. Allan, D. G. Desbruyeres, P. Hyder, C. Liu, and D. Smith, 2017: Surface flux and ocean heat transport convergence contributions to seasonal and interannual variations of ocean heat content. *Journal of Geophysical Research: Oceans*, **122 (1)**, 726–744.

Saravanan, R., and P. Chang, 2019: Midlatitude mesoscale ocean-atmosphere interaction and its relevance to S2S prediction. *Sub-Seasonal to Seasonal Prediction*, Elsevier, 183–200.

Siqueira, L., and B. P. Kirtman, 2016: Atlantic near-term climate variability and the role of a resolved gulf stream. *Geophysical Research Letters*, **43 (8)**, 3964–3972.

Small, R. d., and Coauthors, 2008: Air–sea interaction over ocean fronts and eddies. *Dynamics of Atmospheres and Oceans*, **45 (3-4)**, 274–319.

Small, R. J., F. O. Bryan, S. P. Bishop, S. Larson, and R. A. Tomas, 2019a: What Drives Upper-Ocean Temperature Variability in Coupled Climate Models and Observations? *Journal of Climate*, **33 (2)**, 577–596.

Small, R. J., F. O. Bryan, S. P. Bishop, and R. A. Tomas, 2019b: Air–Sea Turbulent Heat Fluxes in Climate Models and Observational Analyses: What Drives Their Variability? *Journal of Climate*, **32 (8)**, 2397–2421.

Smirnov, D., M. Newman, and M. A. Alexander, 2014: Investigating the role of ocean–atmosphere coupling in the North Pacific Ocean. *Journal of climate*, **27 (2)**, 592–606.

Talley, L., 1984: Meridional heat transport in the Pacific Ocean. *Journal of Physical Oceanography*, **14 (2)**, 231–241.

von Storch, J.-S., 2000: Signatures of air–sea interactions in a coupled atmosphere–ocean GCM. *Journal of Climate*, **13 (19)**, 3361–3379.

Accepted for publication in *Journal of Climate*. DOI 10.1175/JCLI-D-21-0184.1.

Wills, R. C., K. C. Armour, D. S. Battisti, and D. L. Hartmann, 2019a: Ocean–atmosphere dynamical coupling fundamental to the Atlantic multidecadal oscillation. *Journal of Climate*, **32 (1)**, 251–272.

Wills, R. C., D. S. Battisti, C. Proistosescu, L. Thompson, D. L. Hartmann, and K. C. Armour, 2019b: Ocean circulation signatures of North Pacific decadal variability. *Geophysical Research Letters*, **46 (3)**, 1690–1701.

Wu, R., B. P. Kirtman, and K. Pegion, 2006: Local air–sea relationship in observations and model simulations. *Journal of climate*, **19 (19)**, 4914–4932.

Yamamoto, A., H. Tatebe, and M. Nonaka, 2020: On the emergence of the Atlantic multidecadal sst signal: a key role of the mixed layer depth variability driven by North Atlantic Oscillation. *Journal of Climate*, **33 (9)**, 3511–3531.

Yan, X., R. Zhang, and T. R. Knutson, 2018: Underestimated AMOC variability and implications for AMV and predictability in CMIP models. *Geophysical Research Letters*, **45 (9)**, 4319–4328.

Yu, L., X. Jin, and R. A. Weller, 2008: Multidecade global flux datasets from the objectively analyzed air-sea fluxes (OAFlux) project: Latent and sensible heat fluxes, ocean evaporation, and related surface meteorological variables. *OAFlux Project Tech. Rep. OA-2008-01.*, **74**.

Zhang, L., and C. Wang, 2013: Multidecadal North Atlantic sea surface temperature and atlantic meridional overturning circulation variability in CMIP5 historical simulations. *Journal of Geophysical Research: Oceans*, **118 (10)**, 5772–5791.

Zhang, R., 2017: On the persistence and coherence of subpolar sea surface temperature and salinity anomalies associated with the Atlantic multidecadal variability. *Geophysical Research Letters*, **44 (15)**, 7865–7875.

Accepted for publication in *Journal of Climate*. DOI 10.1175/JCLI-D-21-0184.1.

Zhang, R., R. Sutton, G. Danabasoglu, Y.-O. Kwon, R. Marsh, S. G. Yeager, D. E. Amrhein, and C. M. Little, 2019: A review of the role of the Atlantic Meridional Overturning Circulation in Atlantic multidecadal variability and associated climate impacts. *Reviews of Geophysics*, **57 (2)**, 316–375.

Zuo, H., M. A. Balmaseda, S. Tietsche, K. Mogensen, and M. Mayer, 2019: The ECMWF operational ensemble reanalysis–analysis system for ocean and sea ice: a description of the system and assessment. *Ocean science*, **15 (3)**, 779–808.

Accepted for publication in *Journal of Climate*. DOI 10.1175/JCLI-D-21-0184.1.

LIST OF TABLES

Accepted for publication in *Journal of Climate*. DOI 10.1175/JCLI-D-21-0184.1.

Model	Forcing	Damping
H	$F_a = Q_s^*$ $F_o = 0$	$\lambda = \lambda_s$
H_{λ_o}	$F_a = Q_s^*$ $F_o = 0$	$\lambda = \lambda_s + \lambda_o$
H_{λ_o, F_o}	$F_a = Q_s^*$ $F_o = Q_o^*$	$\lambda = \lambda_s + \lambda_o$

TABLE 1. Configurations of the simple stochastic climate model. H corresponds to the model with surface heat fluxes only ($F_o = 0$ and $\lambda = \lambda_s$), H_{λ_o} corresponds to the model with oceanic damping ($F_o = 0$ and $\lambda = \lambda_s + \lambda_o$), and H_{λ_o, F_o} corresponds to the model with oceanic forcing and oceanic damping ($F_o = Q_o^*$ and $\lambda = \lambda_s + \lambda_o$).

Accepted for publication in *Journal of Climate*. DOI 10.1175/JCLI-D-21-0184.1.

LIST OF FIGURES

Accepted for publication in *Journal of Climate*. DOI 10.1175/JCLI-D-21-0184.1.

Accepted for publication in *Journal of Climate*. DOI 10.1175/JCLI-D-21-0184.1.

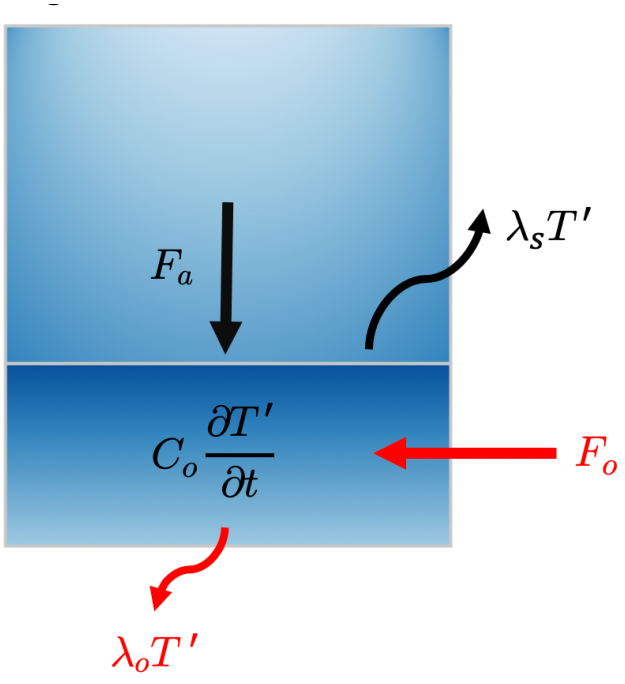

FIG. 1. A schematic of the stochastic climate model with surface heat fluxes only (black terms) and the extension of the model with ocean processes (red terms). F_a is the atmospheric forcing, F_o is the oceanic forcing, λ_s is the surface heat flux damping, λ_o is the ocean dynamical damping, C_o is the mixed-layer heat capacity and T' is the SST anomaly. Each term is described in more detail in the text.

Accepted for publication in *Journal of Climate*. DOI 10.1175/JCLI-D-21-0184.1.

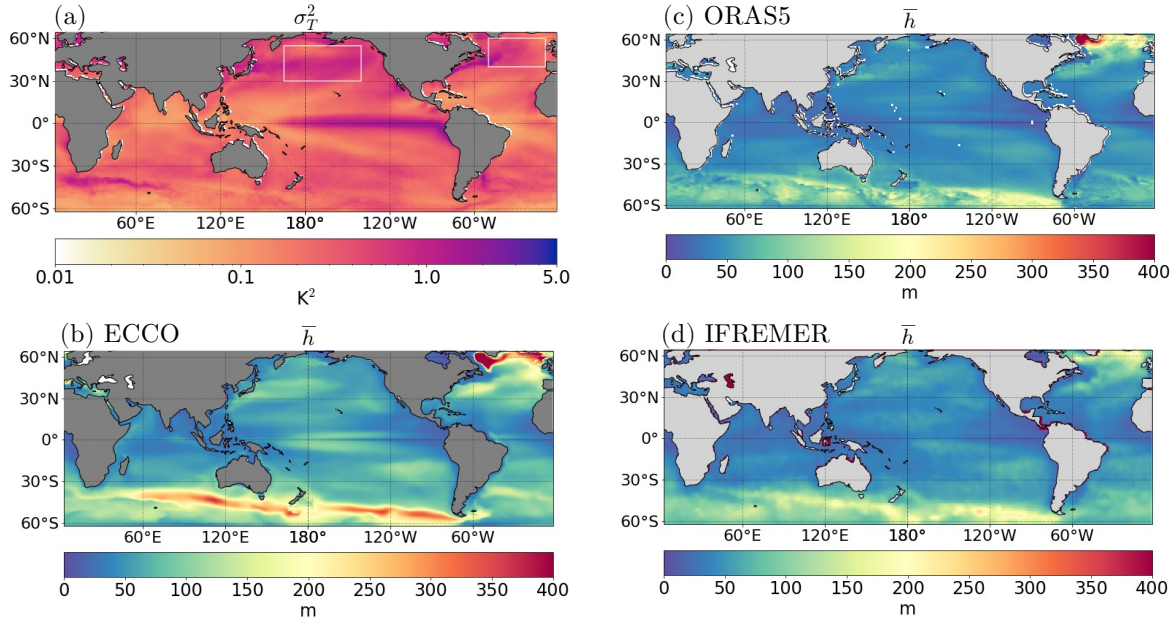

FIG. 2. (a) Observed non-seasonal monthly SST variance (K^2) from OAFlux. The white boxes illustrate the averaging regions used for the analyses. (b) Annual-mean mixed-layer depth (m) from ECCO. (c) Annual-mean mixed-layer depth (m) from ORAS5 ocean reanalysis (d) Observed annual-mean mixed-layer depth from IFREMER.

Accepted for publication in *Journal of Climate*. DOI 10.1175/JCLI-D-21-0184.1.

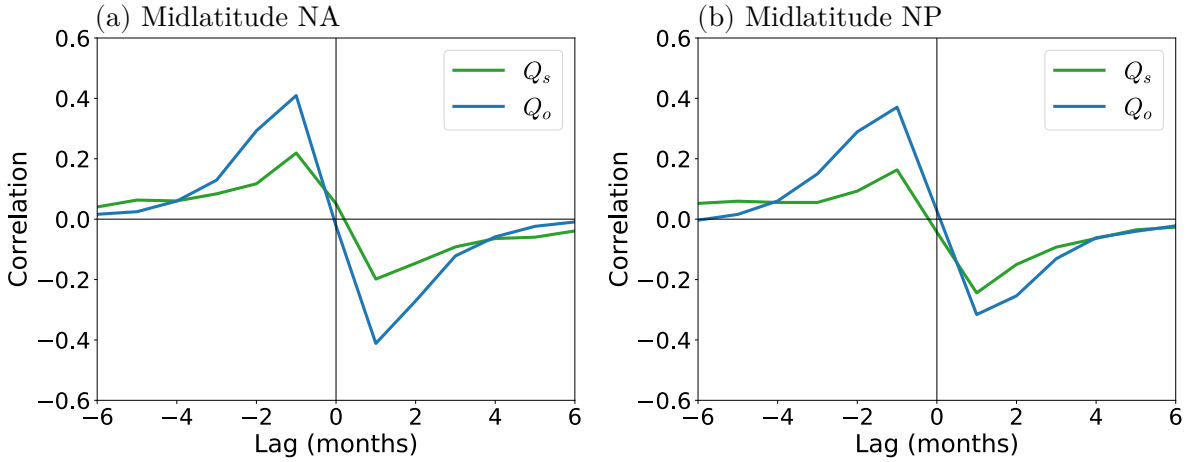

FIG. 3. (a), (b) Lag-correlations between the observed surface heat flux anomalies (Q'_s) and SST anomalies (green), and the observed estimate of ocean heat flux convergence anomalies (Q'_o) and SST anomalies (blue), averaged over the midlatitude North Atlantic region and the midlatitude North Pacific depicted by the boxes in Figure 2a. Negative lag corresponds to the heat fluxes leading the SST anomalies.

Accepted for publication in *Journal of Climate*. DOI 10.1175/JCLI-D-21-0184.1.

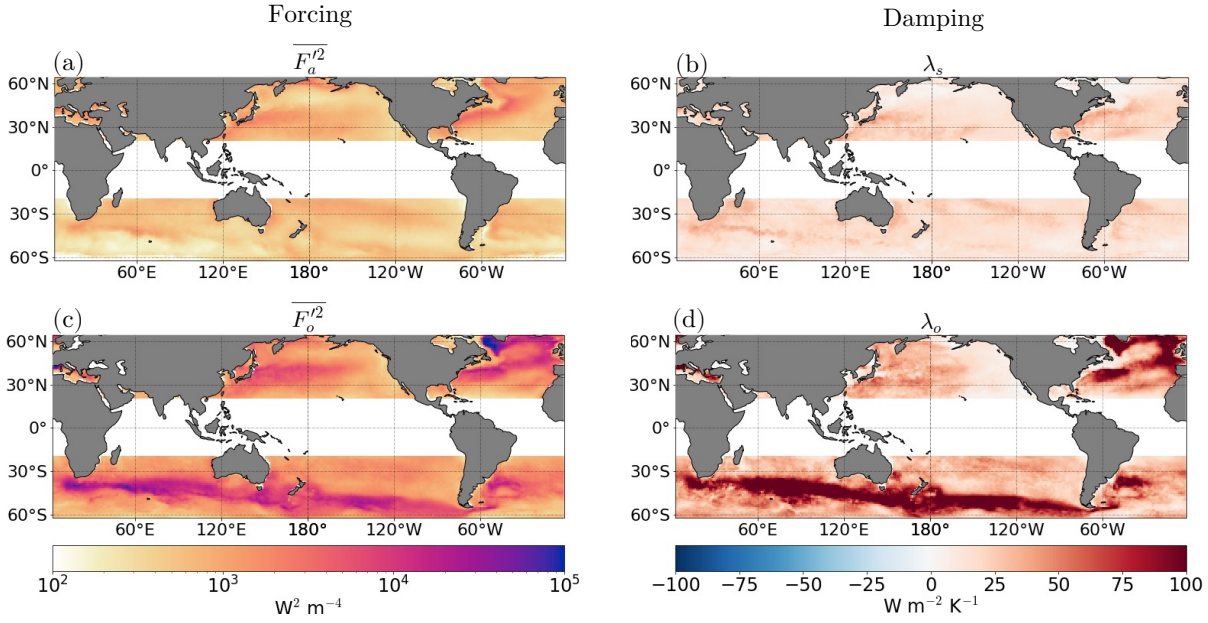

FIG. 4. (a), (c) Monthly variance of the atmospheric forcing and oceanic forcing terms (W^2 m^{-4}). (b), (d) Surface heat flux damping coefficient and oceanic damping coefficient (W m^{-2} K^{-1}). As discussed in Section 2c, tropical regions have been masked because our methods of estimating the forcing and damping terms are not suitable there.

Accepted for publication in *Journal of Climate*. DOI 10.1175/JCLI-D-21-0184.1.

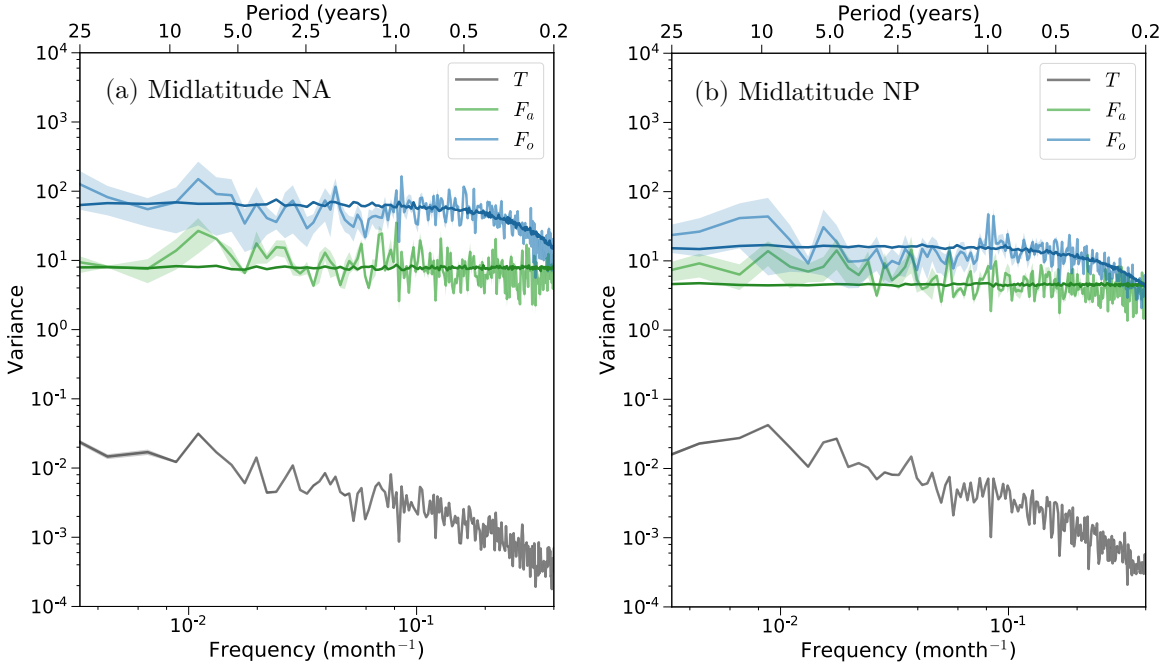

FIG. 5. (a), (b) Power spectra of forcing terms and SST anomalies averaged over the midlatitude North Atlantic and the midlatitude North Pacific for the atmospheric forcing term (green; $W^2\ m^{-4}$), oceanic forcing term (blue; $W^2\ m^{-4}$), and SST anomalies (grey; K^2). Transparent shading indicates uncertainty in the forcing terms, which has been calculated from the error estimates provided by the OAFlux product. The darker green line indicates a white-noise fit to the atmospheric forcing, and the darker blue line indicates a red-noise fit to the oceanic forcing.

Accepted for publication in *Journal of Climate*. DOI 10.1175/JCLI-D-21-0184.1.

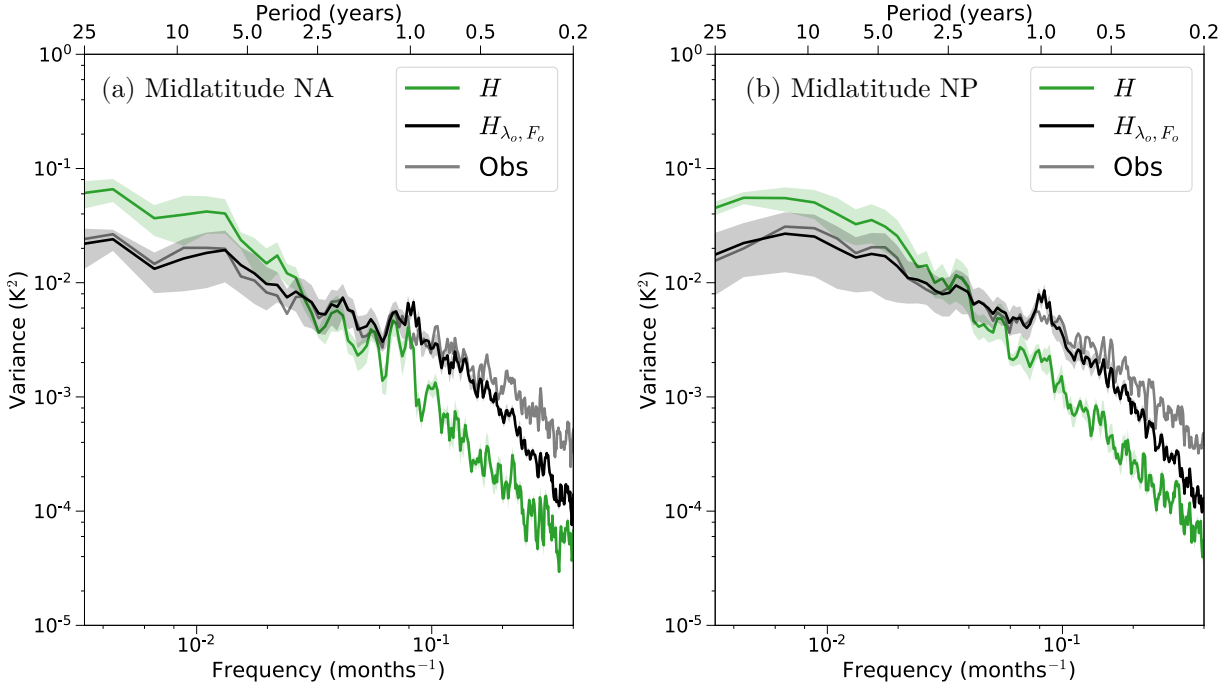

FIG. 6. (a), (b) SST power spectra (K^2) averaged over the midlatitude North Atlantic and North Pacific for the heat flux model (H; green), ocean process model (H_{λ_o,F_o}; black) and observations (grey). Transparent shading indicates uncertainty in the power spectra, which have calculated from the error estimates provided by the OAFlux product. Note that a 3-point average has been applied to the power spectra.

Accepted for publication in *Journal of Climate*. DOI 10.1175/JCLI-D-21-0184.1.

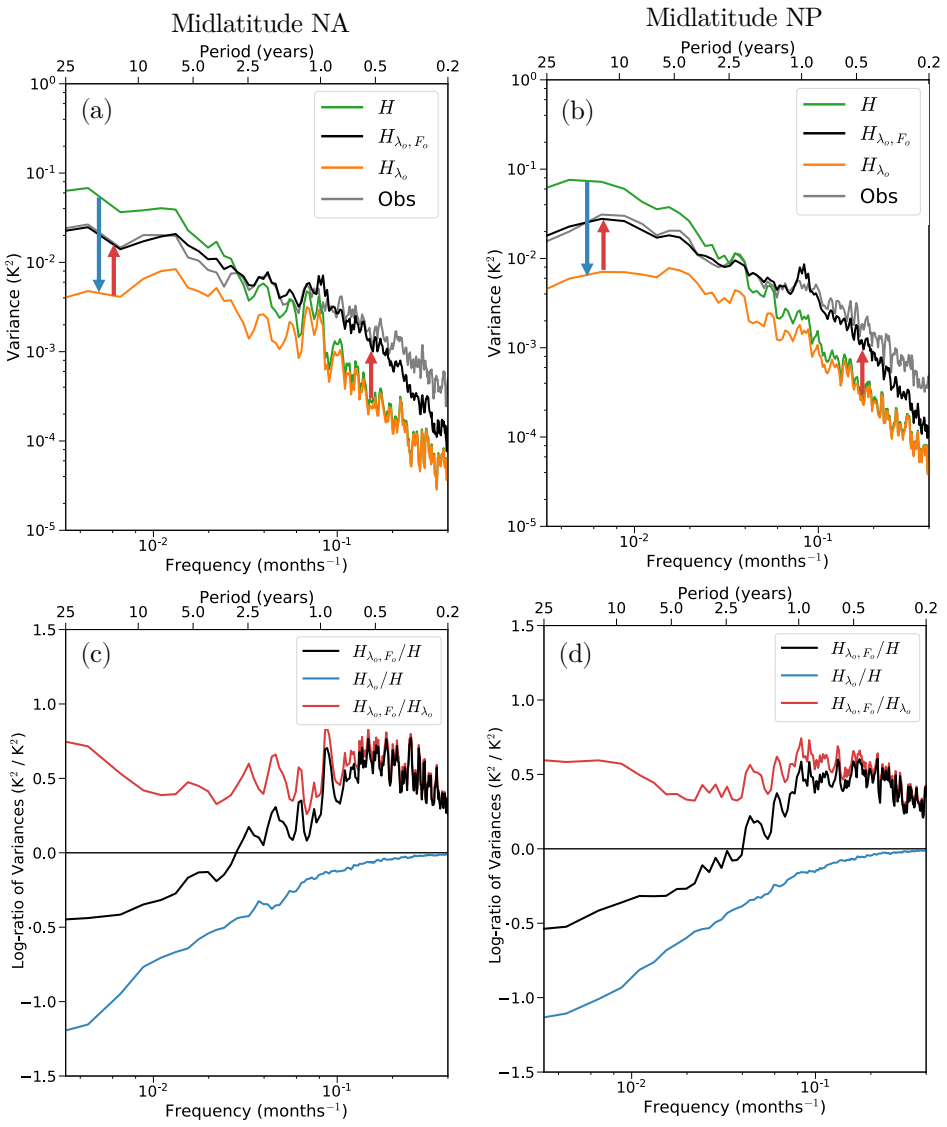

FIG. 7. (a), (b) SST power spectra (K^2) averaged over the midlatitude North Atlantic and midlatitude North Pacific for the heat flux model (H; green), heat flux model with oceanic damping (H_{λ_o}), ocean process model (H_{λ_o,F_o}; black) and observations (grey). The blue arrow in (a) and (b) illustrates the effect of oceanic damping, and the red arrows in (a) and (b) illustrate the effect of oceanic forcing. (c), (d) Log-ratio of the power spectra for various configurations of the simple model for the midlatitude North Atlantic and North Pacific regions. The red line corresponds to $log\left(H_{\lambda_o,F_o}/H_{\lambda_o}\right)$ and hence shows the effect of oceanic forcing as illustrated by the red arrows in (a) and (b). The blue line corresponds to $log\left(H_{\lambda_o}/H\right)$ and hence shows the effect of oceanic damping as illustrated by the blue arrow in (a) and (b). The black line corresponds to $log\left(H_{\lambda_o,F_o}/H\right)$ and hence shows the net effect of oceanic forcing and oceanic damping (i.e., the sum of the red and blue lines).

Accepted for publication in *Journal of Climate*. DOI 10.1175/JCLI-D-21-0184.1.

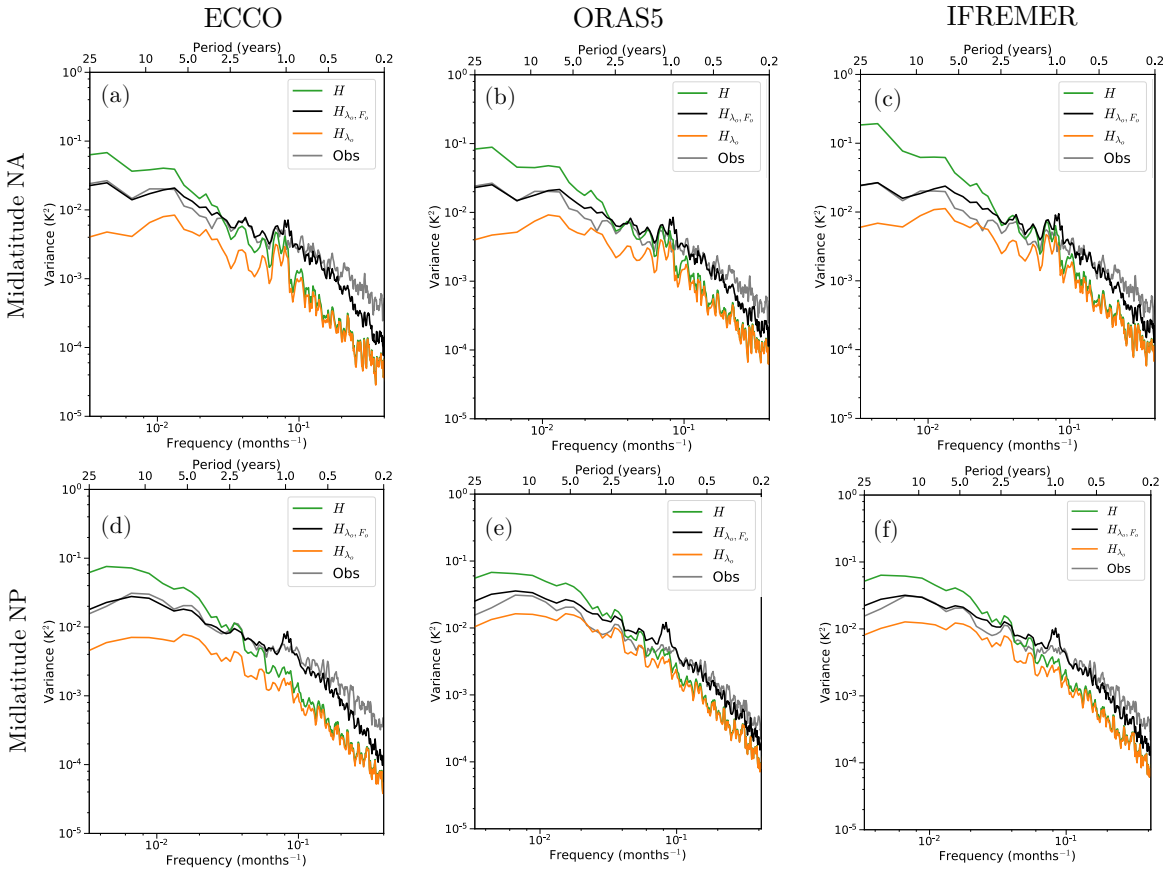

FIG. 8. SST spectra for different model configurations as in Figure 7a,b, except using MLDs from (b,e) ORAS5 reanalysis and (c,f) IFREMER observations. The top row shows spectra averaged over the midlatitude North Atlantic region and the bottom row shows spectra averaged over the midlatitude North Pacific region. Note that the results using (a,d) ECCO MLDs have been reproduced from Figure 7a,b to facilitate comparison between all products.

Accepted for publication in *Journal of Climate*. DOI 10.1175/JCLI-D-21-0184.1.

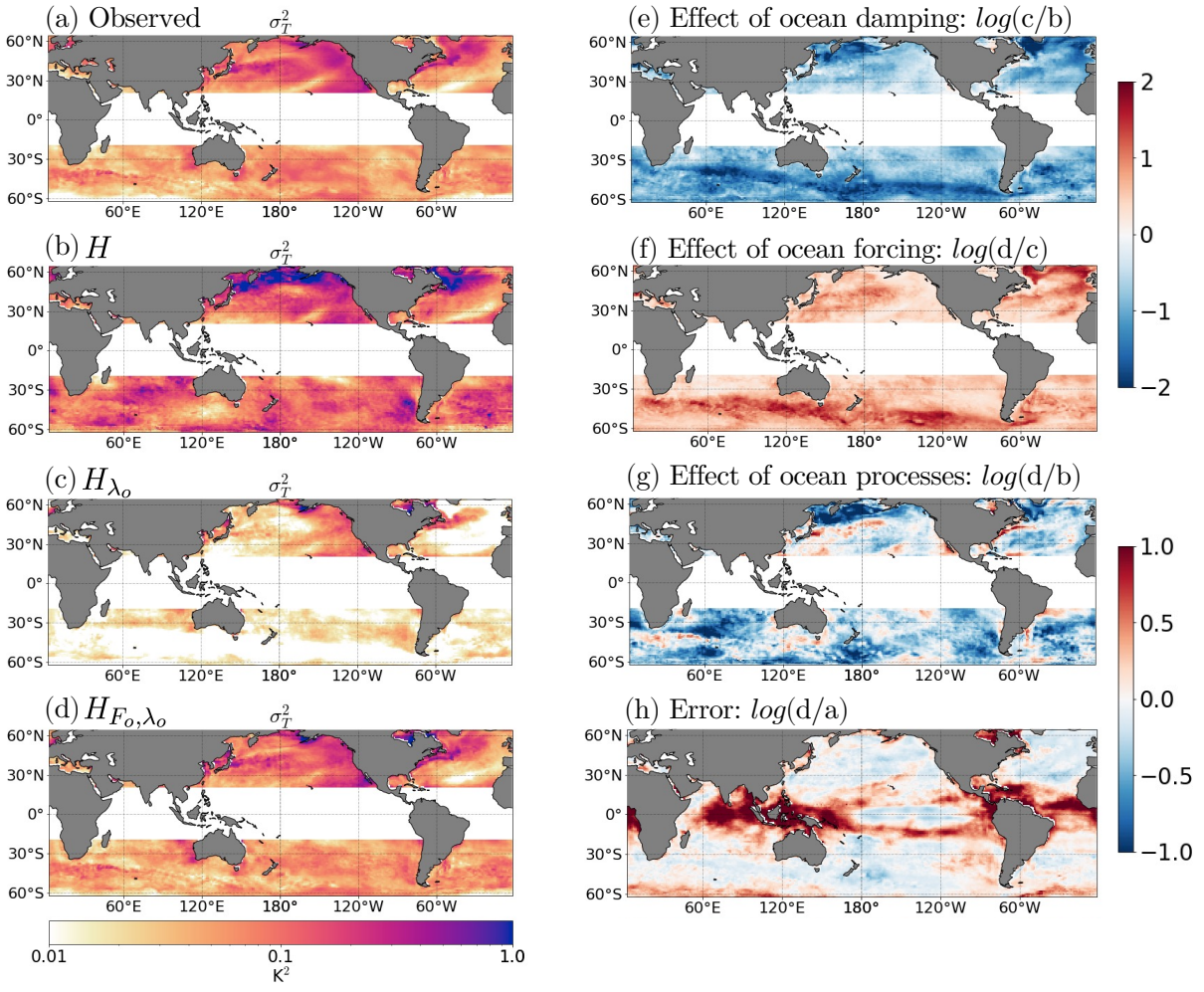

FIG. 9. 5-year low-pass filtered SST variance (K^2) for (a) observations, (b) heat flux model (H), (c) heat flux model with oceanic damping (H_{λ_o}), and (d) ocean process model (H_{λ_o,F_o}). Log-ratio of the 5-year low-pass filtered SST variance for (e) H_{λ_o}/H, i.e., the effects of oceanic damping, (f) $H_{\lambda_o,F_o}/H_{\lambda_o}$, i.e., the effects of oceanic forcing (g) $H_{\lambda_o,F_o}/H$, i.e., the net effects of oceanic forcing and damping, and (h) H_{λ_o,F_o} to the observations, i.e., the error in the ocean process model. Note that the color bar range in (e) and (f) is different than in (g) and (h).

Accepted for publication in *Journal of Climate*. DOI 10.1175/JCLI-D-21-0184.1.

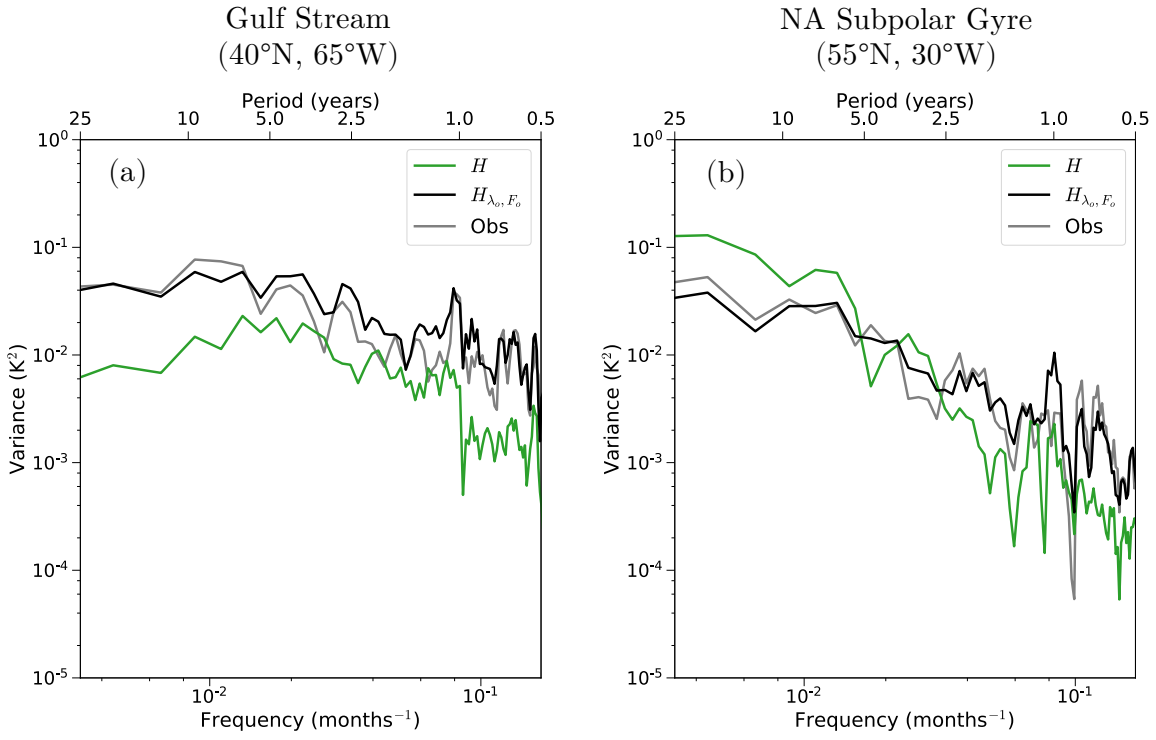

FIG. 10. SST power spectra (K^2) for the heat flux model (H; green), ocean process model (H_{λ_o,F_o}; black) and observations (grey) for a single point in (a) the Gulf Stream current (40°N, 65°W) and (b) interior of the North Atlantic subpolar gyre (55°N, 30°W).

Accepted for publication in *Journal of Climate*. DOI 10.1175/JCLI-D-21-0184.1.

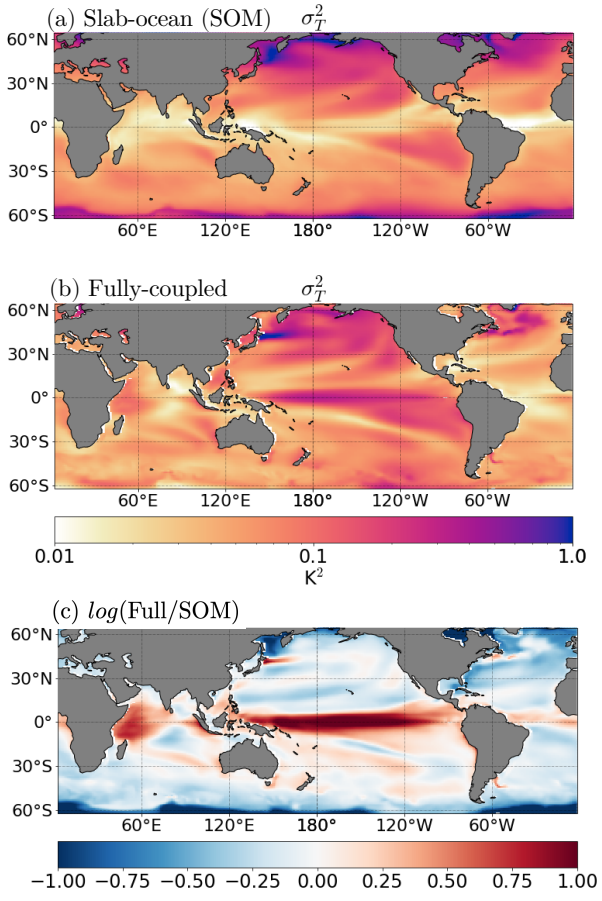

FIG. 11. 5-year low-pass filtered SST variance (K^2) for (a) the slab-ocean model (SOM) configuration of CESM and (b) the fully-coupled configuration of CESM. (c) Log-ratio of the fully-coupled to the SOM 5-year low-pass filtered SST variance, $log\left(\text{Full}/\text{SOM}\right)$.

Accepted for publication in *Journal of Climate*. DOI 10.1175/JCLI-D-21-0184.1.

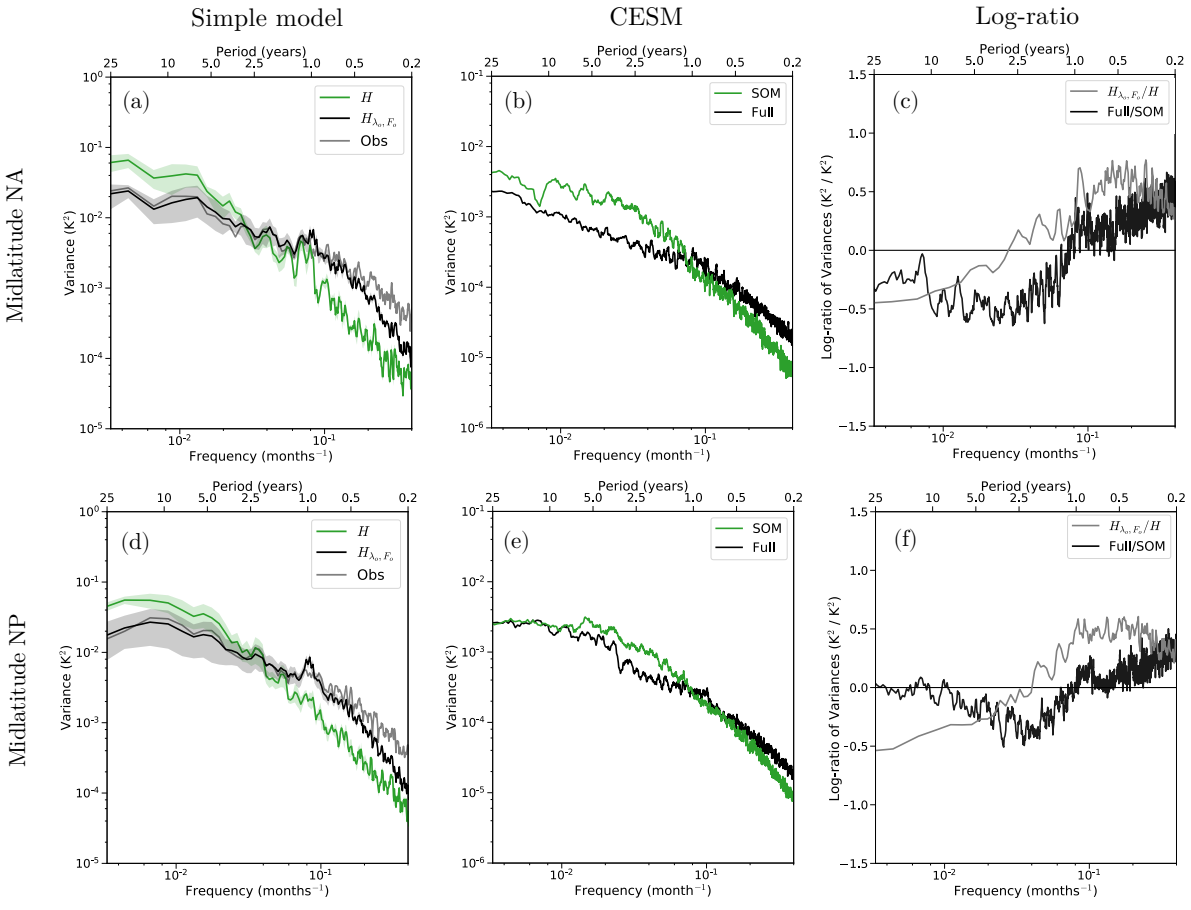

FIG. 12. SST power spectra (K^2) averaged over the midlatitude North Atlantic for (a) the simple model and (b) CESM. Models with ocean dynamical processes are shown in black, and models without ocean dynamical processes are shown in green. (c) Log-ratio of the simulated power spectra with ocean processes to the simulated power spectra without ocean processes for CESM (black) and the simple model (grey). Positive values indicate that ocean dynamical processes increase the power. (d)–(f) As in (a)–(c) except for the midlatitude North Pacific region. Note that a 3-point average has been applied to the simple model power spectra, and a 12-point average has been applied to the CESM power spectra.

Accepted for publication in *Journal of Climate*. DOI 10.1175/JCLI-D-21-0184.1.

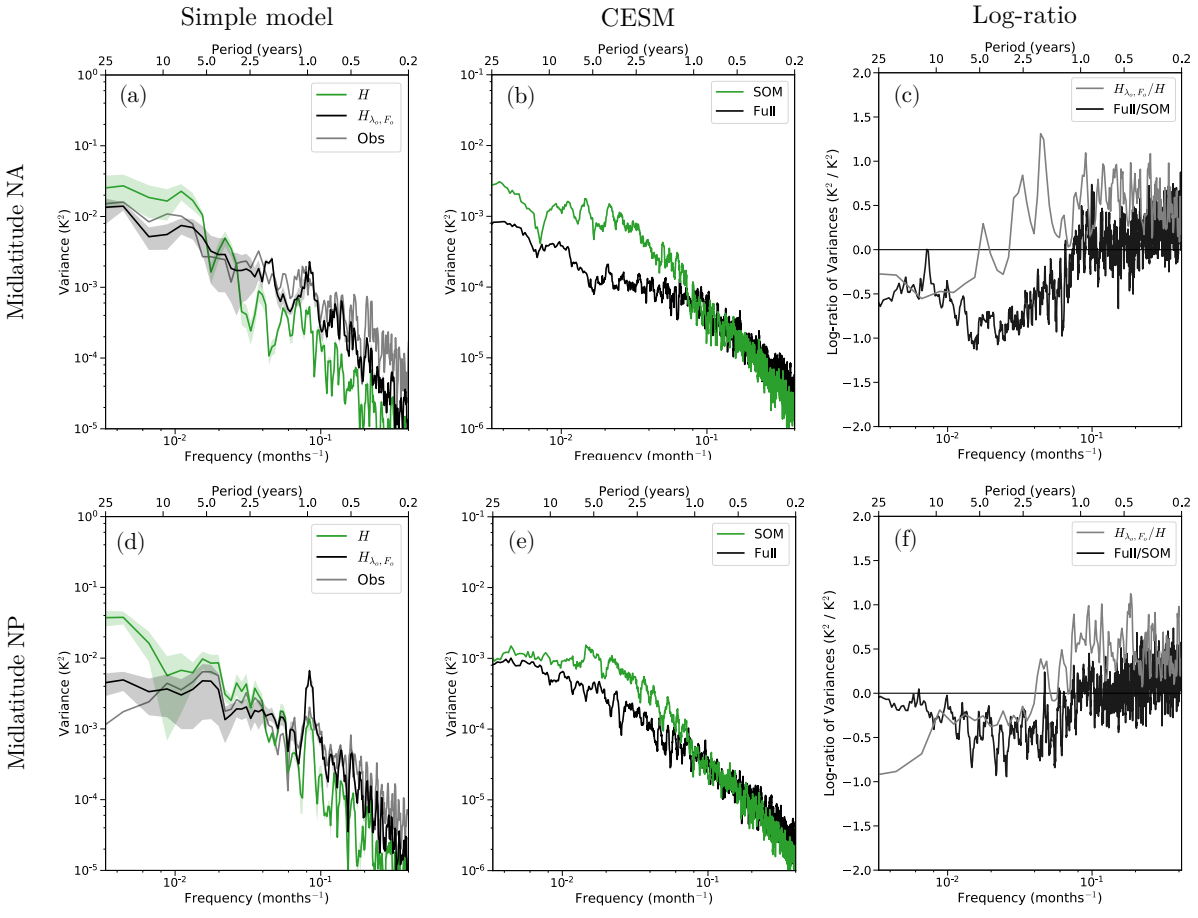

FIG. 13. As in Fig. 11, except the simple model and CESM spectra have been evaluated for (a)-(c) SSTs averaged over the midlatitude North Atlantic region and (d)-(f) SSTs averaged over the midlatitude North Pacific region.

Accepted for publication in *Journal of Climate*. DOI 10.1175/JCLI-D-21-0184.1.

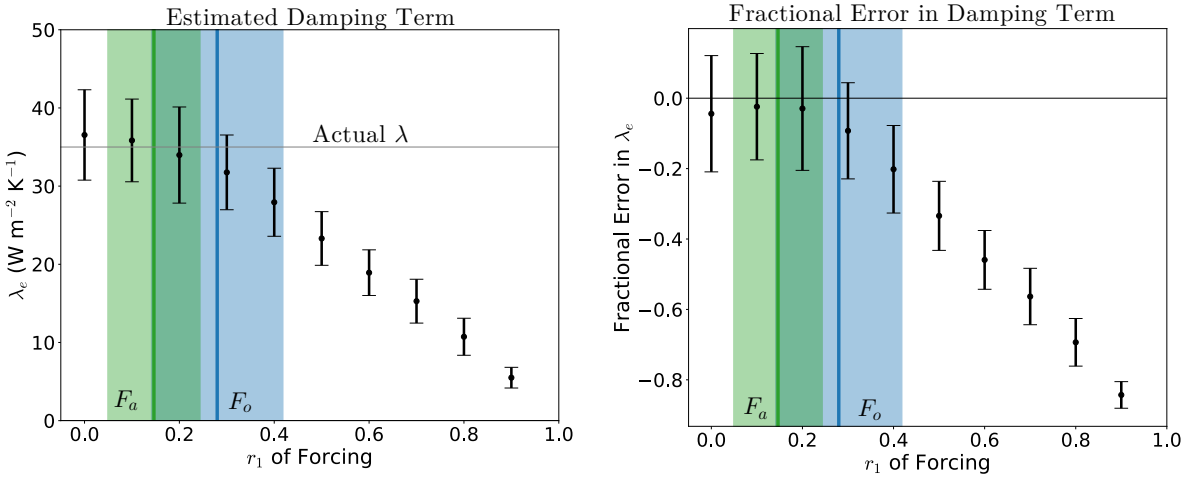

FIG. A1. (Left panel) Estimated damping term (λ_e) as a function of lag-1 autocorrelation (r_1) in the forcing term. (Right panel) Fractional bias in the damping term as a function of r_1 in the forcing term. The procedure for estimating the damping term is described in the Appendix. For each r_1 value, the black dot indicates the mean estimated damping for the 100 different realizations of the red-noise forcing, and the black bars indicate the spread of the estimated damping. The horizontal line indicates the prescribed damping $\lambda = 35$ W m^{-2} K^{-1}. The colored shading indicates the observed ranges of r_1 in the atmospheric forcing term (green) and oceanic forcing term (blue) across all midlatitude points, and the respective colored vertical lines denote the average across all midlatitude points.

Accepted for publication in *Journal of Climate*. DOI 10.1175/JCLI-D-21-0184.1.